Stability Analysis of Primary Plug-and-Play and Secondary Leader-based Controllers for DC Microgrid Clusters

Han, Renke; Tucci, Michele; Martinelli, Andrea; Guerrero, Josep M.; Ferrari-Trecate, Giancarlo

Published in:
IEEE Transactions on Power Systems

DOI (link to publication from Publisher):
10.1109/TPWRS.2018.2884876

Publication date:
2019

Document Version
Accepted author manuscript, peer reviewed version

This article has been accepted for publication in a future issue of this journal, but has not been fully edited. Content may change prior to final publication. Citation information: DOI 10.1109/TPWRS.2018.2884876, IEEE Transactions on Power Systems

Stability Analysis of Primary Plug-and-Play and Secondary Leader-based Controllers for DC Microgrid Clusters

Renke Han, *Member, IEEE,* Michele Tucci, *Member, IEEE,* Andrea Martinelli, Josep M. Guerrero, *Fellow, IEEE,* Giancarlo Ferrari-Trecate, *Senior Member, IEEE*

***Abstract*—In this paper, we propose a new hierarchical control scheme for Microgrid (MG) clusters, given by the interconnection of atomic dc MGs with ZIP loads, each composed by both grid-forming and grid-feeding converters. In the primary level, we develop a new Plug-and-Play (PnP) voltage/current controller in order to achieve simultaneous voltage support and current feeding function with local references. The coefficients of each stabilizing controller are characterized by explicit inequalities, which are related only to local electrical parameters of the MG. Moreover, we provide a sufficient condition on the ZIP loads to guarantee passivity and asymptotic stability of electric system. The robustness of performance to system uncertainties is also demonstrated. In the secondary level, a leader-based voltage/current controller is proposed to achieve both voltage and current regulation for the MG cluster without specifying the individual setpoints for each MG. The proposed distributed controller requires a communication network where each regulator exchanges information with its communication neighbors only. With the proposed scheme, each MG can plug-in/out seamlessly, irrespectively of the power line parameters and models of other MGs. Closed-loop stability proof of MG clusters is formally proved independently of the cluster topology. Moreover, theoretical results are validated by extensive hardware-in-loop (HiL) tests showing robustness of the closed-loop cluster against perturbations in the loads, PnP operations and noises/delays in the communication network.**

***Index Terms*—Plug-and-play, Voltage/Current stability, Grid-Forming/Feeding converters, Leader-based Controller, MG cluster.**

I. Introduction

WITH the increasing penetration of renewable energies into modern electric systems, the concept of MG is receiving increasing attention from both electric industry and academia. A MG is formed by interconnecting a number of renewable energy sources (RESes), energy storage systems (ESSes) and different types of loads [1], [2], [3]. Power converters are the key components applied in both ac and dc MGs to interface different sorts of energy resources and loads to the system. To be specific, in ac MG, power converters can be classified into grid-forming, grid-feeding and grid-supporting converters [4], [5], and the same classification can also be applied for dc MGs. While remarkable progresses have been made in improving the performance of ac MGs during the past decade, dc MGs (which are studied in this paper) have been recognized more and more attractive due to higher efficiency, and more natural interfaces to many types of RESes and ESSes [6], [7].

Grid-forming converters are used as the interface between ESSes and the system to provide voltage support in dc MGs by using voltage-current double loop controller [8]. Further, to achieve simultaneous voltage support and communication-less current sharing among grid-supporting converters, voltage-current (V-I) droop control [1] is widely adopted by imposing virtual impedance for output voltages. However, voltage deviations and current sharing errors still exist due to different line impedances. Another key challenge is that the stability of connected ESSes is sensitive to the chosen virtual impedances which should be designed taking into account the specific MG topology and the line impedances [9], [10]. Recently, an alternative class of decentralized primary controllers, called PnP controller according to the terminology used in [11], has been proposed in [12], [13], [14] for grid-forming converters. In [13] and [14], to achieve PnP voltage control, information about line impedances should be known in order to design local controller. On the other hand, PnP controllers in [13] form a decentralized control architecture where each regulator can be synthesized using information about the corresponding ESSes only [13] or, at most particular parameters of the power lines connected to the ESSes [12]. To be specific, the latter pieces of information are not required in the design procedure of [13] which is therefore termed line-independent.

However, for the PnP methods mentioned above, the synthesis of a local controller requires to solve a convex optimization problem: if unfeasible, the plug-in/out of corresponding ESS must be denied. Moreover, they are only suited to grid-forming converters for providing voltage support in the system. However, one complete MG must be composed of RESes, ESSes and loads to comprise the power generation, storage and consumption. When RESes such as PV sources are included in dc MGs, grid-feeding converters should be used as the interface to achieve current feeding for the system according to the reference given by e.g. maximum power point tracking (MPPT) algorithm [15]. Furthermore current stabilization should be guaranteed [16]. In [17], a current-based PI primary

R. Han is with the Department of Engineering Science, University of Oxford, OX5 1PF, Oxford, United Kingdom. E-mail: renke.han@eng.ox.ac.uk. (Corresponding author)

A. Martinelli is with Automatic Control Laboratory, ETH Zürich, 8092, Zürich, Switzerland.

J. M. Guerrero is with Department of Energy Technology, Aalborg University, 9220, Aalborg, Denmark.

G. Ferrari is with Automatic Control Laboratory, École Polytechnique Fédérale de Lausanne (EPFL), 1015 Lausanne, Switzerland.

This article has been accepted for publication in a future issue of this journal, but has not been fully edited. Content may change prior to final publication. Citation information: DOI 10.1109/TPWRS.2018.2884876, IEEE Transactions on Power Systems

droop control is proposed considering constant current loads. In practical applications, grid-feeding converters should be operated with grid-forming converters to compose a MG. While literature [18], [19] considered the problem of energy management operation between RESes and ESSes, the stability problem about MG with grid-forming/feeding converters and its clusters have always been ignored from system level. On the top of that, distributed secondary controllers, such as [10], [20], [21], mainly focus on the current sharing and balanced voltage regulation only among grid-supporting converters. The stability proof and control parameters design are dependent on the system topology.

In this paper, we define a MG as the combination of a grid-forming and a grid-feeding converters, and study MG clusters arising from the interconnection of MGs. We propose a PnP voltage/current primary controller to achieve grid-forming/feeding function simultaneously. The coefficients of local stabilized controllers are explicitly characterized through a set of inequalities which only depends on the local parameters. Hence, controller design is always feasible and does not require to solve an optimization problem. For MG clusters, a leader-based voltage/current distributed secondary controller is proposed to achieve both voltage and current regulation without specifying separate setpoints for each MG. In order to compute the secondary action, each MG only requires information from its neighbors, defined according to the communication network graph. Differently from [22] where the interface between primary and secondary control is provided by an integral controller, we use PI controller to improve performance during transients. Finally, we provide a proof of the closed-loop stability of MG clusters. The contents of the paper and the main results are summarized in Fig. 1.

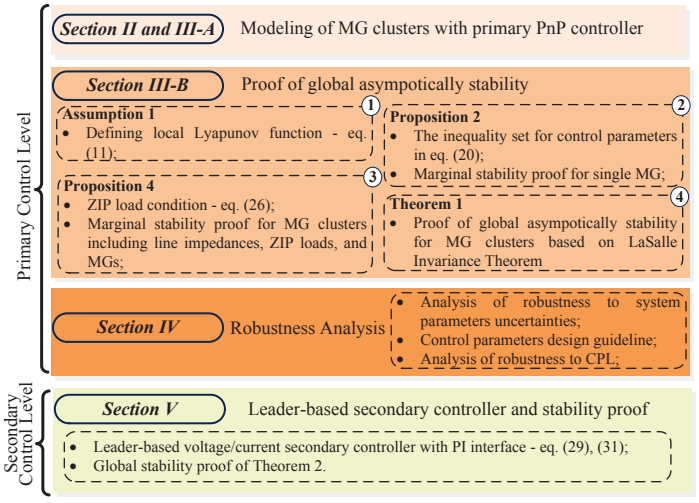

Fig. 1: Flow chart for the content structure.

The paper is structured as follows. In Section II and III-A, the model of MG and proposed voltage/current PnP controller are introduced. In Section III-B, the closed-loop stability for MG clusters with interconnected MGs is proven. In Section IV, robustness analyses to system and control uncertainties are studied and guidelines for designing control parameters are provided. The leader-based voltage/current distributed secondary controller and its stability proof are introduced in Section V. Finally, the HiL tests including system uncertainties test, voltage/current tracking performance test, PnP function test, CPL capacity, and communication delay/noise situations are described in Section VI.

II. DC MG with Grid-Forming/Feeding Converters

A. Electrical model of MGs

We consider a MG composed of one grid-forming converter and one grid-feeding converter connected to the point of common coupling (PCC) bus.

A MG cluster is then obtained by interconnecting N MGs, induced by the set $\mathcal{D} = \{1, \dots, N\}$. Two MGs are neighbors if there is a power line connecting them and denote with $\mathcal{N}_i \subset \mathcal{D}$ the subset of neighbors of MG i. The neighboring relation is symmetric which means $j \in \mathcal{N}_i$ implies $i \in \mathcal{N}_j$. Furthermore, let $\mathcal{E} = \{(i,j) : i \in \mathcal{D},\ j \in \mathcal{N}_i\}$ collect unordered pairs of indices associated to lines. The topology of the MG cluster is then described by the undirected graph $\mathcal{G}_{el}$ with nodes $\mathcal{D}$ and edges $\mathcal{E}$.

At each PCC bus, a ZIP load including constant impedance load (CIL), constant current load (CCL), and constant power load (CPL), is considered. The ZIP model is illustrated in upper block of Fig. 2 where R_i, I_{CCLi} and P_{CPLi} represents the CIL (Z), CCL (I), and CPL (P) respectively for MG i. Since the goal of grid-forming converter in each MG is to keep the PCC voltage constant, it is reasonable that the CPL in ZIP load are linearized around a voltage operating point V_{op}. Then the equivalent model for CPL, shown in the lower block of Fig. 2, is

$$I_{CPLi} = \underbrace{-\frac{P_{CPLi}}{V_{op}^2} V_i}_{(a)} + \underbrace{2\frac{P_{CPLi}}{V_{op}}}_{(b)} \tag{1}$$

where V_i is i-th PCC voltage, and I_{CPLi} is the total current for CPL i.

In (1), the equivalent CPL consists of two parts including part (a), the negative impedance part which can undermine stability of the system and part (b), the constant current load which cannot affect stability of the system.

In total, the ZIP load can be represented by one equivalent impedance load R_{Li} given by the parallel interconnection of R_i, and the equivalent negative impedance $(-\frac{V_{op}^2}{P_{CPLi}})$, and one equivalent current load given by the sum of CCL I_{CCLi} and the equivalent CCL $(2\frac{P_{CPLi}}{V_{op}})$ due to CPL. In formulae, it can be written as

$$\begin{cases} R_{Li} = R_i // (-\dfrac{V_{op}^2}{P_{CPLi}}) \\ I_{Li} = I_{CCLi} + 2\dfrac{P_{CPLi}}{V_{op}} \end{cases} \tag{2}$$

The electrical scheme of the i-th MG is provided by left block of Fig. 3. The corresponding model is

$$\text{MG } i : \begin{cases} \dfrac{dV_i}{dt} = \dfrac{1}{C_{ti}} I_{ti}^C + \dfrac{1}{C_{ti}} I_{ti}^V + \displaystyle\sum_{j \in \mathcal{N}_i} \left(\frac{V_j}{C_{ti} R_{ij}} - \frac{V_i}{C_{ti} R_{ij}} \right) \\ \qquad\qquad - \dfrac{1}{C_{ti}} (I_{Li} + \dfrac{V_i}{R_{Li}}) \\ \dfrac{dI_{ti}^C}{dt} = -\dfrac{1}{L_{ti}^C} V_i - \dfrac{R_{ti}^C}{L_{ti}^C} I_{ti}^C + \dfrac{1}{L_{ti}^C} V_{ti}^C \\ \dfrac{dI_{ti}^V}{dt} = -\dfrac{1}{L_{ti}^V} V_i - \dfrac{R_{ti}^V}{L_{ti}^V} I_{ti}^V + \dfrac{1}{L_{ti}^V} V_{ti}^V \end{cases} \tag{3}$$

This article has been accepted for publication in a future issue of this journal, but has not been fully edited. Content may change prior to final publication. Citation information: DOI 10.1109/TPWRS.2018.2884876, IEEE Transactions on Power Systems

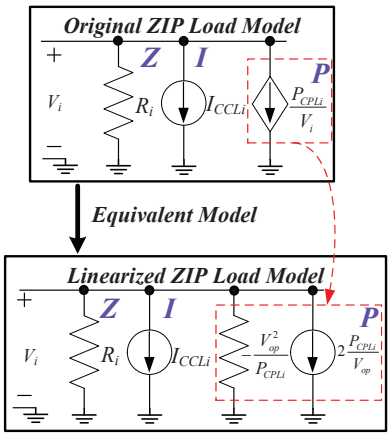

Fig. 2: Equivalent linearized ZIP model.

where variables V_i, I_{ti}^C, I_{ti}^V are the i-th PCC voltage, filter current from RES and filter current from ESS, respectively. For the grid-feeding converter, V_{ti}^C represents the command and R_{ti}^C, L_{ti}^C are the electrical parameters. For the grid-forming converter, V_{ti}^V represents the command and R_{ti}^V, L_{ti}^V are the electrical parameters; C_{ti} is the capacitor at the PCC bus. Moreover, V_j is the voltage at the PCC of each neighboring MGs $j \in \mathcal{N}_i$ and R_{ij} and L_{ij} are the resistance and inductance of the dc power line connecting MGs i and j. In general, the RL parameters are different for grid-feeding and grid-forming converters.

B. State-space model of a MG Cluster

Dynamics (3) provides the state-space model:

$$\Sigma_{[i]}^{MG}: \begin{cases} \dot{x}_{[i]}(t) = A_{ii}x_{[i]}(t) + B_i u_{[i]}(t) + M_i d_{[i]}(t) \\ \qquad\quad + \xi_{[i]}(t) + A_{load,i}x_{[i]}(t) \\ z_{[i]}(t) = H_i x_{[i]}(t) \end{cases}$$

where $x_{[i]} = [V_i, I_{ti}^C, I_{ti}^V]^T$ is the state of the system, $u_{[i]} = [V_{ti}^C, V_{ti}^V]$ is the control input, $d_{[i]} = I_{Li}$ is the exogenous input and $z_{[i]} = [I_i^C, V_i]$ is the controlled variable. The term $\xi_{[i]} = \sum_{j\in\mathcal{N}_i} A_{ij}(x_{[j]} - x_{[i]})$ accounts for the coupling with each MG $j \in \mathcal{N}_i$. The matrices of $\Sigma_{[i]}^{MG}$ are obtained from (3) as:

$$A_{ii} = \begin{bmatrix} 0 & \frac{1}{C_{ti}} & \frac{1}{C_{ti}} \\ -\frac{1}{L_{ti}^C} & -\frac{R_{ti}^C}{L_{ti}^C} & 0 \\ -\frac{1}{L_{ti}^V} & 0 & -\frac{R_{ti}^V}{L_{ti}^V} \end{bmatrix}, A_{load,i} = \begin{bmatrix} -\frac{1}{R_{Li}C_{ti}} & 0 & 0 \\ 0 & 0 & 0 \\ 0 & 0 & 0 \end{bmatrix}, M_i = \begin{bmatrix} -\frac{1}{C_{ti}} \\ 0 \\ 0 \end{bmatrix},$$

$$A_{ij} = \begin{bmatrix} \frac{1}{R_{ij}C_{ti}} & 0 & 0 \\ 0 & 0 & 0 \\ 0 & 0 & 0 \end{bmatrix}, B_i = \begin{bmatrix} 0 & 0 \\ \frac{1}{L_{ti}^C} & 0 \\ 0 & \frac{1}{L_{ti}^V} \end{bmatrix}, H_i = \begin{bmatrix} 0 & 1 & 0 \\ 1 & 0 & 0 \end{bmatrix}.$$

The overall model for a MG cluster is given by

$$\begin{aligned} \dot{\mathbf{x}}(t) &= \mathbf{A}\mathbf{x}(t) + \mathbf{B}\mathbf{u}(t) + \mathbf{M}\mathbf{d}(t) \\ \mathbf{z}(t) &= \mathbf{H}\mathbf{x}(t) \end{aligned} \tag{4}$$

where $\mathbf{x} = (x_{[1]}, \ldots, x_{[N]}) \in \mathbb{R}^{3N}$, $\mathbf{u} = (u_{[1]}, \ldots, u_{[N]}) \in \mathbb{R}^{2N}$, $\mathbf{d} = (d_{[1]}, \ldots, d_{[N]}) \in \mathbb{R}^{N}$, $\mathbf{z} = (z_{[1]}, \ldots, z_{[N]}) \in \mathbb{R}^{2N}$. The blocks composing matrices $\mathbf{A}$, $\mathbf{B}$, $\mathbf{M}$, $\mathbf{H}$ are given in (5) shown in the upper part of next page.

III. Design of Stabilizing Primary Voltage/Current Controllers

A. Structure of PnP Voltage/Current controllers

In order to track constant references $\mathbf{z_{ref}}(t)$, when $\mathbf{d}(t)$ is constant as well, the MG model is augmented with integrators [23]. A necessary condition for making error $\mathbf{e}(t) = \mathbf{z_{ref}}(t) - \mathbf{z}(t)$ equal to zero as $t \to \infty$, is that, for arbitrary $\bar{\mathbf{d}}$ and $\bar{\mathbf{z}}_{\mathbf{ref}}$, there are equilibrium states and inputs $\bar{\mathbf{x}}$ and $\bar{\mathbf{u}}$ verifying (4). The existence of these equilibrium points can be shown as in the proof of Proposition 1 in [12].

Let $I_{cap,i} > 0$ define the maximal output current capability that can be provided by MG i. According to the block on the middle bottom of Fig. 3, the dynamics of integrators are given by

$$\begin{cases} \dot{v}_{[i]}^C(t) = e_{[i]}^C(t) = z_{ref_{[i]}}^{Pri,C}(t) - I_{ti}^C(t) & \text{(6a)} \\ \dot{v}_{[i]}^V(t) = e_{[i]}^V(t) = z_{ref_{[i]}}^{Pri,V}(t) - V_i(t) & \text{(6b)} \end{cases}$$

where $z_{ref_{[i]}}^{Pri,C} = I_{ref,i}^{Pri,pu} * I_{cap,i}$, $z_{ref_{[i]}}^{Pri,V} = V_{ref,i}^{Pri}$,

Hence, the augmented MG model is

$$\hat{\Sigma}_{[i]}^{MG}: \begin{cases} \dot{\hat{x}}_{[i]}(t) = \hat{A}_{ii}\hat{x}_{[i]}(t) + \hat{B}_i u_{[i]}(t) + \hat{M}_i \hat{d}_{[i]}(t) \\ \qquad\quad + \hat{\xi}_{[i]}(t) + \hat{A}_{load,i}\hat{x}_{[i]}(t) \\ z_{[i]}(t) = \hat{H}_i \hat{x}_{[i]}(t) \end{cases} \tag{7}$$

where $\hat{x}_{[i]} = [V_i, I_{ti}^C, v_i^C, I_{ti}^V, v_i^V]^T \in \mathbb{R}^5$ is the state, $\hat{d}_{[i]} = [d_{[i]}, z_{ref_{[i]}}^{Pri,C}, z_{ref_{[i]}}^{Pri,V}]^T \in \mathbb{R}^3$ collects the exogenous signals and $\hat{\xi}_{[i]} = \sum_{j\in\mathcal{N}_i} \hat{A}_{ij}(\hat{x}_{[j]} - \hat{x}_{[i]})$. Matrices in (7) are defined as follows

$$\hat{A}_{ii} = \begin{bmatrix} 0 & \frac{1}{C_{ti}} & 0 & \frac{1}{C_{ti}} & 0 \\ -\frac{1}{L_{ti}^C} & -\frac{R_{ti}^C}{L_{ti}^C} & 0 & 0 & 0 \\ 0 & -1 & 0 & 0 & 0 \\ -\frac{1}{L_{ti}^V} & 0 & 0 & -\frac{R_{ti}^V}{L_{ti}^V} & 0 \\ -1 & 0 & 0 & 0 & 0 \end{bmatrix}, \hat{B}_i = \begin{bmatrix} 0 & 0 \\ \frac{1}{L_{ti}^C} & 0 \\ 0 & 0 \\ 0 & \frac{1}{L_{ti}^V} \\ 0 & 0 \end{bmatrix},$$

$$\hat{M}_i = \begin{bmatrix} -\frac{1}{C_{ti}} & 0 & 0 \\ 0 & 0 & 0 \\ 0 & 1 & 0 \\ 0 & 0 & 0 \\ 0 & 0 & 1 \end{bmatrix}, \hat{A}_{ij} = \begin{bmatrix} A_{ij} & \mathbf{0}_{3\times 2} \\ \mathbf{0}_{2\times 3} & \mathbf{0}_{2\times 2} \end{bmatrix},$$

$$\hat{A}_{load,i} = \begin{bmatrix} A_{load,i} & \mathbf{0}_{3\times 2} \\ \mathbf{0}_{2\times 3} & \mathbf{0}_{2\times 2} \end{bmatrix}, \hat{H}_i = \begin{bmatrix} H_i & \mathbf{0}_{2\times 2} \end{bmatrix}.$$

Based on Proposition 2 in [12], it can be proven that the pair $(\hat{A}_{ii}, \hat{B}_i)$ is controllable. Hence, system (7) can be stabilized. The overall augmented system is obtained from (7) as

$$\begin{cases} \dot{\hat{\mathbf{x}}}(t) = \hat{\mathbf{A}}\hat{\mathbf{x}}(t) + \hat{\mathbf{B}}\mathbf{u}(t) + \hat{\mathbf{M}}\hat{\mathbf{d}}(t) \\ \mathbf{z}(t) = \hat{\mathbf{H}}\hat{\mathbf{x}}(t) \end{cases} \tag{8}$$

where $\hat{\mathbf{x}}$ and $\hat{\mathbf{d}}$ collect variables $\hat{x}_{[i]}$ and $\hat{d}_{[i]}$ respectively, and matrices $\hat{\mathbf{A}}, \hat{\mathbf{B}}, \hat{\mathbf{M}}$ and $\hat{\mathbf{H}}$ are obtained from systems (7).

Each MG $\hat{\Sigma}_{[i]}^{MG}$ is with the following state-feedback controller

$$\mathcal{C}_{[i]}^{MG}: \qquad u_{[i]}(t) = K_i \hat{x}_{[i]}(t) \tag{9}$$

where

$$K_i = \begin{bmatrix} k_{1,i}^C & k_{2,i}^C & k_{3,i}^C & 0 & 0 \\ k_{1,i}^V & 0 & 0 & k_{2,i}^V & k_{3,i}^V \end{bmatrix} \in \mathbb{R}^{2\times 5}.$$

Note that the control variables V_{ti}^C and V_{ti}^V are coupled through the coefficients $k_{1,i}^C$ and $k_{1,i}^V$ appearing in the first column of K_i. In other words, measurement of V_i are used

This article has been accepted for publication in a future issue of this journal, but has not been fully edited. Content may change prior to final publication. Citation information: DOI 10.1109/TPWRS.2018.2884876, IEEE Transactions on Power Systems

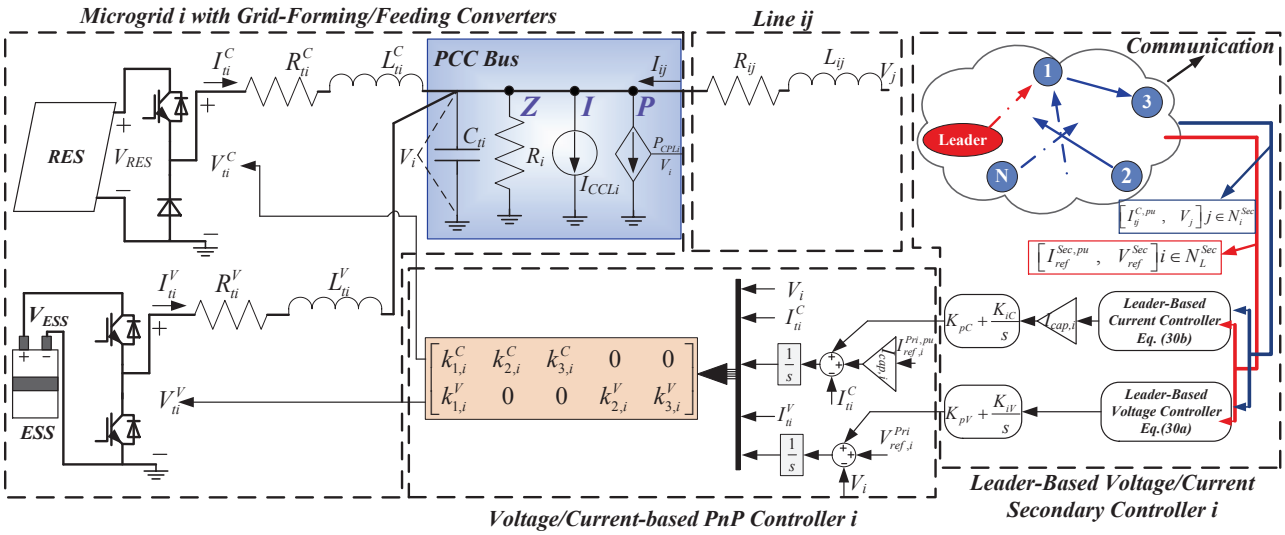

Fig. 3: Electrical scheme of MG i with hierarchical PnP voltage/current controller.

$$\mathbf{A}=\begin{bmatrix} A_{11}+A_{load,1} & A_{12} & A_{13} & \dots & A_{1N} \\ A_{21} & A_{22}+A_{load,2} & A_{23} & \dots & A_{2N} \\ A_{31} & A_{32} & A_{33}+A_{load,3} & \dots & A_{3N} \\ \vdots & \vdots & \vdots & \ddots & \vdots \\ A_{N1} & A_{N2} & A_{N3} & \dots & A_{NN}+A_{load,N} \end{bmatrix},$$

$$\mathbf{B}=\begin{bmatrix} B_1 & 0 & \dots & 0 \\ 0 & B_2 & \ddots & \vdots \\ \vdots & \ddots & \ddots & 0 \\ 0 & \dots & 0 & B_N \end{bmatrix},\ \mathbf{M}=\begin{bmatrix} M_1 & 0 & \dots & 0 \\ 0 & M_2 & \ddots & \vdots \\ \vdots & \ddots & \ddots & 0 \\ 0 & \dots & 0 & M_N \end{bmatrix},\ \mathbf{H}=\begin{bmatrix} H_1 & 0 & 0 & \dots & 0 \\ 0 & H_2 & 0 & \ddots & \vdots \\ 0 & 0 & H_3 & \ddots & 0 \\ \vdots & \ddots & \ddots & \ddots & 0 \\ 0 & \dots & 0 & 0 & H_N \end{bmatrix}. \tag{5}$$

for generating both V_{ti}^C and V_{ti}^V. In particular, the overall control architecture is decentralized since the computation of $u_{[i]}$ requires the state of $\hat{\Sigma}_{[i]}^{MG}$ only.

B. Conditions for stability of the closed-loop MG Cluster

For showing stability, we will use local Lyapunov functions

$$V_i(\hat{x}_{[i]})=[\hat{x}_{[i]}]^T P_i \hat{x}_{[i]}. \tag{10}$$

Assumption 1. *The positive definite matrix $P_i \in \mathbb{R}^{5\times 5}$ in (10) fulfills*

$$P_i=\left[\begin{array}{c|cc} \eta_i & \mathbf{0}_{1\times 2} & \mathbf{0}_{1\times 2} \\ \hline \mathbf{0}_{2\times 1} & \mathcal{P}_{22,i}^C & \mathbf{0}_{2\times 2} \\ \hline \mathbf{0}_{2\times 1} & \mathbf{0}_{2\times 2} & \mathcal{P}_{44,i}^V \end{array}\right], \tag{11}$$

where

$$\mathcal{P}_{22,i}^C=\begin{bmatrix} p_{22,i}^C & p_{23,i}^C \\ p_{23,i}^C & p_{33,i}^C \end{bmatrix}, \mathcal{P}_{44,i}^V=\begin{bmatrix} p_{44,i}^V & p_{45,i}^V \\ p_{54,i}^V & p_{55,i}^V \end{bmatrix}. \tag{12}$$

And $\eta_i>0$ is a local parameter satisfying $\eta_i=\bar{\sigma}C_{ti}$, $i\in\mathcal{D}$ where $\bar{\sigma}>0$ is a constant parameter, common to all MGs.

In absence of coupling terms $\hat{\xi}_{[i]}(t)$, and load terms $\hat{A}_{load,i}\hat{x}_{[i]}(t)$, we would like to guarantee asymptotic stability of the nominal closed-loop MG

$$\dot{\hat{x}}_{[i]}(t)=\underbrace{(\hat{A}_{ii}+\hat{B}_i K_i)}_{F_i}\hat{x}_{[i]}(t)+\hat{M}_i\hat{d}_{[i]}(t). \tag{13}$$

By direct calculation, one can show that F_i has the following structure

$$\begin{aligned} F_i &= \left[\begin{array}{c|c|c|c} 0 & f_{12,i} & 0 & f_{14,i} \ \ 0 \\ \hline f_{21,i} & f_{22,i} & f_{23,i} & 0 \ \ 0 \\ 0 & f_{32,i} & 0 & 0 \ \ 0 \\ \hline f_{41,i} & 0 & 0 & f_{44,i} \ \ f_{45,i} \\ f_{51,i} & 0 & 0 & 0 \ \ 0 \end{array}\right] \\ &= \left[\begin{array}{c|c|c|c} 0 & \frac{1}{C_{ti}} & 0 & \frac{1}{C_{ti}} \ \ 0 \\ \hline \frac{(k_{1,i}^C-1)}{L_{ti}^C} & \frac{(k_{2,i}^C-R_{ti}^C)}{L_{ti}^C} & \frac{k_{3,i}^C}{L_{ti}^C} & 0 \ \ 0 \\ 0 & -1 & 0 & 0 \ \ 0 \\ \hline \frac{(k_{1,i}^V-1)}{L_{ti}^V} & 0 & 0 & \frac{(k_{2,i}^V-R_{ti}^V)}{L_{ti}^V} \ \ \frac{k_{3,i}^V}{L_{ti}^V} \\ -1 & 0 & 0 & 0 \ \ 0 \end{array}\right] \\ &= \left[\begin{array}{c|c|c} 0 & \mathcal{F}_{12,i}^C & \mathcal{F}_{14,i}^V \\ \hline \mathcal{F}_{21,i}^C & \mathcal{F}_{22,i}^C & 0 \\ \hline \mathcal{F}_{41,i}^V & 0 & \mathcal{F}_{44,i}^V \end{array}\right]. \end{aligned} \tag{14}$$

From Lyapunov theory, asymptotic stability of (13) can be certified by the existence of a Lyapunov function $\mathcal{V}_i(\hat{x}_{[i]})=$

This article has been accepted for publication in a future issue of this journal, but has not been fully edited. Content may change prior to final publication. Citation information: DOI 10.1109/TPWRS.2018.2884876, IEEE Transactions on Power Systems

$[\hat{x}_{[i]}]^T P_i \hat{x}_{[i]}$ where $P_i = P_i^T > 0$ and

$$Q_i = F_i^T P_i + P_i F_i \tag{15}$$

is negative definite. In presence of nonzero coupling terms, we will show that asymptotic stability can be achieved under Assumption 1.

Based on (11) and (14), (15) can be rewritten as (16) shown in the upper part of the next page.

Next, we provide a number of results, whose proof is shown in Appendix, enabling one to prove the main result about the controller design provided by Theorem 1.

Proposition 1. *[13] If $Q = Q^T \leq 0$ and an element q_{ii} on the diagonal verifies $q_{ii} = 0$, then*

(i) The matrix Q cannot be negative definite.

(ii) The i-th row and column of Q have zero entries.

Lemma 1. *Under Assumption 1, if $Q_i \leq 0$, Q_i has the following structure*

$$Q_i = \left[\begin{array}{c|c|c} 0 & \mathbf{0}_{1\times 2} & \mathbf{0}_{1\times 2} \\ \hline \mathbf{0}_{2\times 1} & \mathcal{Q}_{22,i}^C & \mathbf{0}_{2\times 2} \\ \hline \mathbf{0}_{2\times 1} & \mathbf{0}_{2\times 2} & \mathcal{Q}_{44,i}^V \end{array}\right] \tag{17}$$

Furthermore, the blocks on the diagonal verify

$$\begin{cases} \mathcal{Q}_{22,i}^C \leq 0 & \text{(18a)} \\ \mathcal{Q}_{44,i}^V \leq 0 & \text{(18b)} \end{cases}$$

Remark 1. *The MG considered is not restricted to only two DGs in one MG: the proof can be extended to $(\mathcal{N} + \mathcal{M}) \in \mathbb{R}$ DGs for each MG where $\mathcal{N} \in \mathbb{R}$ represents the number of grid-feeding DGs and $\mathcal{M} \in \mathbb{R}$ represents the number of grid-forming DGs. In terms of the proof, we can augment the proposed Lyapunov matrix by adding new diagonal blocks. The generalized Lyapunov matrix is defined as* (19) *shown on upper part of the next page. To be noticed, for each sub-matrix, the subscript does not represent the dimension of the sub-matrix, which is only used to distinguish the different matrice. Then the proof can just follow the step in this paper.*

Remark 2. *Since the blocks $\mathcal{Q}_{22,i}^C$ and $\mathcal{Q}_{44,i}^V$ belong to $\mathbb{R}^{2\times 2}$, from* (18)*, it has that the determinants of $\mathcal{Q}_{22,i}^C$ and $\mathcal{Q}_{44,i}^V$ are nonnegative.*

Proposition 2. *Under Assumption 1, P_i and Q_i have the* (20) *shown in the upper part of next page , where $h_i = L_{ti}^V k_{3,i}^V - (k_{1,i}^V - 1)(k_{2,i}^V - R_{ti}^V)$. Moreover, if $P_i > 0$, $Q_i \leq 0$ and $Q_i \neq 0$, one has*

$$\begin{cases} k_{1,i}^C < 1 \\ k_{2,i}^C < R_{ti}^C \\ k_{3,i}^C > 0 \end{cases}, \quad \begin{cases} k_{1,i}^V < 1 \\ k_{2,i}^V < R_{ti}^V \\ 0 < k_{3,i}^V < \frac{1}{L_{ti}^V}(k_{1,i}^V - 1)(k_{2,i}^V - R_{ti}^V) \end{cases} \tag{21}$$

Lemma 2. *Let Assumption 1 and Proposition 2 hold. Let us define $h_i(v_i) = v_i^T \mathcal{Q}_{44,i}^V v_i$, with $v_i \in \mathbb{R}^2$. If $Q_i \leq 0$, and $Q_i \neq 0$, then*

$$h_i(\bar{v}_i) = 0 \Longleftrightarrow \bar{v}_i \in \mathrm{Ker}(\mathcal{F}_{44,i}^V).$$

Proposition 3. *Let $g_i(w_i) = w_i^T Q_i w_i$, $\forall i \in \mathcal{D}$ with $w_i \in \mathbb{R}^5$. Under Assumption 1, Proposition 2, and Lemma 2, only vectors $\bar{w}_i$ in the form*

$$\bar{w}_i = \left[\begin{array}{ccccc} \alpha_i & 0 & \gamma_i & \beta_i & \delta_i\beta_i \end{array}\right]^T$$

with α_i, γ_i, $\beta_i \in \mathbb{R}$, and $\delta_i = -\frac{k_{2,i}^V - R_{ti}^V}{k_{3,i}^V}$, fulfill

$$g_i(\bar{w}_i) = \bar{w}_i^T Q_i \bar{w}_i = 0. \tag{22}$$

Consider the overall closed-loop MG cluster model

$$\begin{cases} \dot{\hat{\mathbf{x}}}(t) = (\hat{\mathbf{A}} + \hat{\mathbf{B}}\mathbf{K})\hat{\mathbf{x}}(t) + \hat{\mathbf{M}}\hat{\mathbf{d}}(t) \\ \mathbf{z}(t) = \hat{\mathbf{H}}\hat{\mathbf{x}}(t) \end{cases} \tag{23}$$

obtained by combining (8) and (9), with $\mathbf{K} = \mathrm{diag}(K_1, \ldots, K_N)$. Considering also the collective Lyapunov function

$$\mathcal{V}(\hat{\mathbf{x}}) = \sum_{i=1}^{N} \mathcal{V}_i(\hat{x}_{[i]}) = \hat{\mathbf{x}}^T \mathbf{P} \hat{\mathbf{x}} \tag{24}$$

where $\mathbf{P} = \mathrm{diag}(P_1, \ldots, P_N)$. One has $\dot{\mathcal{V}}(\hat{\mathbf{x}}) = \hat{\mathbf{x}}^T \mathbf{Q} \hat{\mathbf{x}}$ where

$$\mathbf{Q} = (\hat{\mathbf{A}} + \hat{\mathbf{B}}\mathbf{K})^T \mathbf{P} + \mathbf{P}(\hat{\mathbf{A}} + \hat{\mathbf{B}}\mathbf{K}). \tag{25}$$

A consequence of Proposition 1 is that, under Assumption 1, the matrix $\mathbf{Q}$ cannot be negative definite. At most, one has

$$\mathbf{Q} \leq 0. \tag{26}$$

Moreover, even if $Q_i \leq 0$ holds for all $i \in \mathcal{D}$, the inequality (26) might be violated because of the nonzero coupling terms $\hat{A}_{ij}$ and load terms $\hat{A}_{load,i}$ in matrix $\hat{\mathbf{A}}$. The next proposition shows that this cannot happen.

Proposition 4. *If gains K_i are chosen according to* (21)*, and the CIL R_i and CPL P_{CPLi} in the ZIP load for each MG verify*

$$P_{CPLi} \leq \frac{V_{op}^2}{R_i}, \tag{27}$$

then $Q_i \leq 0$. Moreover, if (27) *holds $\forall i \in \mathcal{D}$, then* (26) *holds.*

Theorem 1. *If Assumption 1 is fulfilled, the graph $\mathcal{G}_{el}$ is connected, ZIP loads satisfy* (27)*, and control coefficients are chosen according to* (21)*, then the origin of* (8) *is asymptotically stable.*

The proofs of Lemma 1 and 2, Proposition 2, 3, and 4, Theorem 1 are provided in the Appendix.

Remark 3. *The proof in Appendix D for Proposition 4 shows that if CIL and CPL in ZIP load satisfy inequality* (27)*, the system is stable. From the circuit theory viewpoint, if the inequality* (27) *is not verified, which means the negative impedance due to CPL is larger than the positive impedance of CIL, then the electrical network fails to be passive. If assuming that the controller effects are ignored and the electrical network is considered only under this serious condition, the system will become unstable due to non-passivity. However, the proposed controller for MGs can provide passivity features, which means extra damping are integrated in the system. Thus, if we connect MG equipped with the proposed controllers, even though inequality* (27) *is not verified, the system can also*

This article has been accepted for publication in a future issue of this journal, but has not been fully edited. Content may change prior to final publication. Citation information: DOI 10.1109/TPWRS.2018.2884876, IEEE Transactions on Power Systems

$$Q_i = \begin{bmatrix} 0 & [\mathcal{F}_{21,i}^C]^T\mathcal{P}_{22,i}^C + \eta_i\mathcal{F}_{12,i}^C & [\mathcal{F}_{41,i}^V]^T\mathcal{P}_{44,i}^V + \eta_i\mathcal{F}_{14,i}^V \\ [\mathcal{F}_{12,i}^C]^T\eta_i + \mathcal{P}_{22,i}^C\mathcal{F}_{21,i}^C & [\mathcal{F}_{22,i}^C]^T\mathcal{P}_{22,i}^C + \mathcal{P}_{22,i}^C\mathcal{F}_{22,i}^C & \mathbf{0}_{2\times2} \\ [\mathcal{F}_{14,i}^V]^T\eta_i + \mathcal{P}_{44,i}^V\mathcal{F}_{41,i}^V & \mathbf{0}_{2\times2} & [\mathcal{F}_{44,i}^V]^T\mathcal{P}_{44,i}^V + \mathcal{P}_{44,i}^V\mathcal{F}_{44,i}^V \end{bmatrix} = \begin{bmatrix} 0 & \mathcal{Q}_{12,i}^C & \mathcal{Q}_{14,i}^V \\ [\mathcal{Q}_{12,i}^C]^T & \mathcal{Q}_{22,i}^C & \mathbf{0}_{2\times2} \\ [\mathcal{Q}_{14,i}^V]^T & \mathbf{0}_{2\times2} & \mathcal{Q}_{44,i}^V \end{bmatrix} \tag{16}$$

$$P_i = \begin{bmatrix} \eta_i & \mathbf{0}_{1\times2} & \cdots & \mathbf{0}_{1\times2} & \cdots & \cdots & \cdots \\ \mathbf{0}_{2\times1} & \mathcal{P}_{22,i}^C & \mathbf{0}_{2\times2} & \cdots & \cdots & \cdots & \cdots \\ \vdots & \mathbf{0}_{2\times2} & \ddots & \mathbf{0}_{2\times2} & \cdots & \cdots & \cdots \\ \vdots & \vdots & \mathbf{0}_{2\times2} & \mathcal{P}_{2\mathcal{N}*2\mathcal{N},i}^C & \mathbf{0}_{2\times2} & \cdots & \cdots \\ \vdots & \vdots & \vdots & \mathbf{0}_{2\times2} & \mathcal{P}_{(2\mathcal{N}+2)*(2\mathcal{N}+2),i}^V & \mathbf{0}_{2\times2} & \cdots \\ \vdots & \vdots & \vdots & \vdots & \mathbf{0}_{2\times2} & \ddots & \mathbf{0}_{2\times2} \\ \vdots & \vdots & \vdots & \vdots & \vdots & \mathbf{0}_{2\times2} & \mathcal{P}_{2\mathcal{M}*2\mathcal{M},i}^V \end{bmatrix}. \tag{19}$$

$$P_i = \begin{bmatrix} \eta_i & 0 & 0 & 0 & 0 \\ 0 & p_{22,i}^C & 0 & 0 & 0 \\ 0 & 0 & \frac{k_{3,i}^C}{L_{ti}^C}p_{22,i}^C & 0 & 0 \\ 0 & 0 & 0 & \frac{L_{ti}^V}{C_{ti}}\frac{(k_{2,i}^V - R_{ti}^V)}{h_i} & \frac{L_{ti}^V}{C_{ti}}\frac{k_{3,i}^V}{h_i} \\ 0 & 0 & 0 & \frac{L_{ti}^V}{C_{ti}}\frac{k_{3,i}^V}{h_i} & \frac{1}{C_{ti}}\frac{k_{3,i}^V(k_{1,i}^V-1)}{h_i} \end{bmatrix}, Q_i = \begin{bmatrix} 0 & 0 & 0 & 0 & 0 \\ 0 & 2\frac{(k_{2,i}^C - R_{ti}^C)}{L_{ti}^C}p_{22,i}^C & 0 & 0 & 0 \\ 0 & 0 & 0 & 0 & 0 \\ 0 & 0 & 0 & 2\frac{(k_{2,i}^V - R_{ti}^V)^2}{C_{ti}h_i} & 2\frac{(k_{2,i}^V - R_{ti}^V)k_{3,i}^V}{C_{ti}h_i} \\ 0 & 0 & 0 & 2\frac{(k_{2,i}^V - R_{ti}^V)k_{3,i}^V}{C_{ti}h_i} & 2\frac{(k_{3,i}^V)^2}{C_{ti}h_i} \end{bmatrix} \tag{20}$$

survive with tolerance to a certain degree. The intuitive robust analysis about ZIP load and a detailed passivity analysis of the system output impedance will be given in subsection IV-C by root locus analysis and bode diagram. The HiL test in section VI-D will also be given to verify the passive effectiveness of proposed controllers and the accuracy of theoretical results.

Remark 4. *The design of stabilizing controller for each MG can be conducted according to Proposition 2. In particular, differently from the approach in [13], no optimization problem has to be solved for computing a local controller. Indeed, it is enough to choose control coefficient $k_{1,i}^C$, $k_{2,i}^C$, $k_{3,i}^C$ and $k_{1,i}^V$, $k_{2,i}^V$, $k_{3,i}^V$ fulfilling the inequalities in* (21)*. Note that these inequalities are always feasible, implying that a stabilizing controller always exists. Moreover, the inequalities depend only on the parameters R_{ti}^C and R_{ti}^V of the MG i. Therefore, the control synthesis is independent of parameters of MGs and power lines, which means that controller design can be executed only once for each converter in a plug-and play fashion. From Theorem 1, local controllers also guarantee stability of the whole MG cluster. When new MGs are plugged in the MG cluster, if their controllers are designed as described above, the stability of the new MG cluster can be guaranteed by Theorem 1 (notice that the new graph $\mathcal{G}_{el}$ is connected by construction). Instead, when a MG is plugged out, the electrical graph $\mathcal{G}_{el}$ might be disconnected and split into two connected graphs. Yet, Theorem 1 can still be applied to show the stability of each sub-cluster.*

IV. Robustness Analysis

In this section, we will analyze robustness of stability to system uncertainties, control parameters and ZIP load variations. Moreover, the passivity features induced by the proposed controllers are shown, hence demonstrating that they provide extra damping, hence extending the system stability margin for CPLs. For convenience, in the following analyses, an MG cluster consisting of two MGs is considered, and the system and controller parameters are same as those in Section VI, (See in Table I and II). The analyses below are based on closed-loop system model given in (8).

A. Robustness to system parameters uncertainties

The inequalities (21) depend only on the parameters R_{ti}^C and R_{ti}^V of the MG i which are the equivalent resistance of filter inductors. If they cannot be known exactly, one can just set a tolerance percentage $\sigma_i \in [0, 1]$ in (21), which can be rewritten as

$$\begin{cases} k_{1,i}^C < 1 \\ k_{2,i}^C < (1-\sigma_i)R_{ti}^C \\ k_{3,i}^C > 0 \end{cases}, \quad \begin{cases} k_{1,i}^V < 1 \\ k_{2,i}^V < (1-\sigma_i)R_{ti}^V \\ 0 < k_{3,i}^V < \frac{1}{L_{ti}^V}(k_{1,i}^V - 1)(k_{2,i}^V - R_{ti}^V). \end{cases} \tag{28}$$

Moreover, since the equivalent resistance of inductors cannot be negative, we can just choose $k_{2,i}^C$ and $k_{2,i}^V$ to be less than zero to guarantee stability of the whole system, which works for all parameter uncertainties.

To further prove the robustness to uncertainties of system parameters, Fig. 4 shows the pole-zero locus obtained by changing the values of capacitors C_{ti}, inductors L_{ti}^C and the equivalent resistances R_{ti}^C for grid-feeding converters, inductors L_{ti}^V and the equivalent resistances R_{ti}^V for grid-forming converters respectively. The control parameters are kept invariant when the system parameters are changed. One can

This article has been accepted for publication in a future issue of this journal, but has not been fully edited. Content may change prior to final publication. Citation information: DOI 10.1109/TPWRS.2018.2884876, IEEE Transactions on Power Systems

notice that even though the system parameters are changed, the whole system can be kept stable by using the same control parameters.

B. Robustness to control parameters

In this subsection, we discuss pole-zero locus in Fig. 5 which are obtained by changing the control parameters within the stable range. It is proved again that if the inequalities (21) are satisfied, all the poles of the closed-loop system are located in the right half plane (RHP) and the stability of the system can be guaranteed. Furthermore, the locus of poles can also provide guidelines for choosing the controller parameters so as to improve the dynamic performance of the system.

C. Robustness to load parameters

This analysis is divided into two parts. Firstly, one MG is considered. The CIL in ZIP load is set as $R_i = 20\ \Omega$. According to the results given in Proposition 4, the system might become unstable when P_{CPLi} becomes larger than $48^2/20 = 115.2W$. In this analysis, the power of CPL P_{CPLi} is changed from 0 W to 680 W. As shown in Fig. 6, the system can still be stable until P_{CPLi} become $610W$, after which one pair of poles goes into the RHP. The result shows that except for the damping from CIL, the proposed controller can provide extra damping to compensate the negative impedance due to CPL. In particular, from the model given in (8), the bode diagram profile between V_i and I_{Li} called the closed-loop system output impedance [24], [25], [26] is shown in Fig. 7. Since the phase margin is between 90 and -90 degree within the whole frequency range, the system output impedance is passive, which means it provides extra damping to the system.

To further illustrate effectiveness of the extra damping induced by the proposed controller, an MG cluster consisting of two MGs is considered. The test condition is same as before, but the power of CPL is changed from 0 W to 1000 W. The pole-zero locus in Fig. 8 shows that the system is stable within the larger power range than before. It is because more MGs are connected into the system, more extra damping is provided and then the whole system can supply more CPL than before. The analysis results will be further proved in the HiL test in Section VI-D.

D. Region of Attraction

We would like to show that the PnP controller can provide a large region of attraction (ROA). Based on the original nonlinear model, we tested the stability and convergence of system with different initial states. Since the CPL is linearized at the voltage operating point, we considered the following two initial voltage conditions with $200W$ CPL power.

In the first scenario, the initial voltage is chosen as $-1V$. Normally, the voltage is started at $0V$ initial value and finally tracking $48V$ with no steady errors, thus negative initial voltage state is a challenge to be handled. Then the state trajectory is shown in Fig. 9. The x-axis represents the current tracking error $e^C_{[i]}(t)$ and the y-axis represents the voltage tracking error $e^V_{[i]}(t)$. The red circle represents the equilibrium point. It can be seen in Fig. 9 that even if the system starts from the negative initial voltage value, a stable behavior is obtained. In total, there are five states for each MG. Since the voltage and current tracking errors converge to zero, the integrated error states $v^C_{[i]}(t)$ and $v^V_{[i]}(t)$ converge to constant values. Further, the current from grid-forming converter is also stable due to the stable voltage performance.

In the second scenario, the initial voltage is chosen as $120V$, i.e. an initial voltage value that is much higher than the nominal one. The simulation result is given in Fig. 10 which shows the tracking errors also converge to zero also in this case.

The test shows that the system has a large region of attraction which can make the system safe even under large disturbance or start-up stage.

V. Design of Stabilizing Leader-based Secondary Controllers for a MG cluster

The proposed primary PnP controller can achieve both the voltage and current tracking with the local references for each MG. However, to achieve the coordination within MG clusters, references should be provided by the upper control layer to achieve voltage tracking and current sharing reasonably. Furthermore, to avoid using a centralized controller to send the reference value for each PnP controller, a leader-based distributed controller is proposed in the secondary layer including leader-based voltage and current controllers. In particular, references are provided only to the leader node and then they will be diffused through the MG thanks to the consensus scheme.

A. Leader-based Voltage/Current Secondary Controller

The proposed secondary controller has the goal of sharing information about reference signals in a distributed way.

Based on (13) and (14), the transfer function from voltage reference $z^{Pri,V}_{ref_{[i]}}$ and current reference $z^{Pri,C}_{ref_{[i]}}$ to output voltage V_i and output current I^C_{ti} can be written as $\hat{H}_i(sI - \hat{F}_i)\tilde{M}_i$ where $\tilde{M}_i$ collects the second and third columns of $\hat{M}_i$. Setting $s = 0$, the identity matrix is obtained which means the primary PnP control loops can be approximated by unit-gain relations

$$\begin{cases} V_i = V^{Pri}_{ref,i} & \text{(29a)} \\ \dfrac{I^C_{ti}}{I_{cap,i}} = I^{C,pu}_{ti} = I^{Pri,pu}_{ref,i} & \text{(29b)} \end{cases}$$

The secondary control layer exploits a communication network linking MGs and fulfilling the following Assumption.

Assumption 2. *The communication graph $\mathcal{G}^{Sec} = (\mathcal{D}, \mathcal{E}^{Sec})$ is connected and undirected implying that communication links within a MG cluster are bidirectional. Over each communication link $(i, j) \in \mathcal{E}^{Sec}$, the pairs of variables $(I^{C,pu}_{ti}, V_i)$ and $(I^{C,pu}_{tj}, V_j)$ are transmitted. Furthermore, the graph $\mathcal{G}^{Sec}$ is endowed with an additional node termed the leader node, carrying the reference values $(I^{Sec,pu}_{ref}, V^{Sec}_{ref})$ and connected to at least one node belongs to $\mathcal{D}$.*

This article has been accepted for publication in a future issue of this journal, but has not been fully edited. Content may change prior to final publication. Citation information: DOI 10.1109/TPWRS.2018.2884876, IEEE Transactions on Power Systems

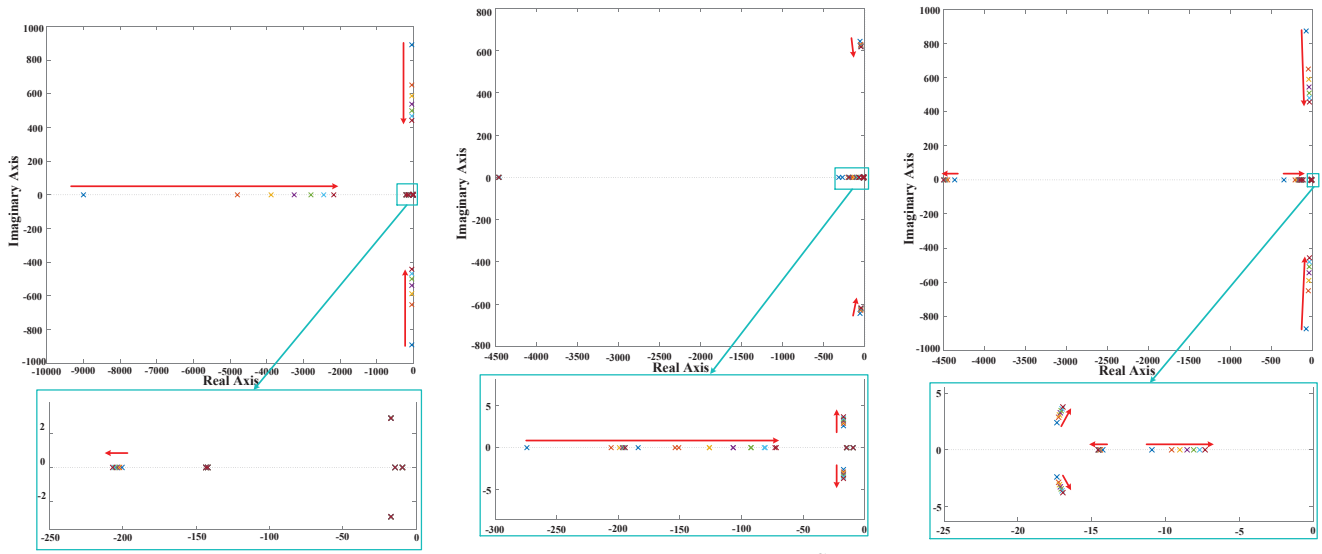

(a) Pole-zero locus by changing C_{ti} from 1.1 mF to 4.4 mF.

(b) Pole-zero locus by changing L_{ti}^{C} from 0.009 H to 0.036 H and R_{ti}^{C} from 0.1 Ω to 0.4 Ω.

(c) Pole-zero locus by changing L_{ti}^{V} from 0.0009 H to 0.0036 H and R_{ti}^{V} from 0.05 Ω to 0.2 Ω.

Fig. 4: Robustness analyses to system parameters.

The proposed leader-based voltage and current distributed secondary controller can be written as:

$$\begin{cases} e_{Vi} = \sum\limits_{j\in\mathcal{N}_i^{Sec}} a_{ij}\left(V_i - V_j\right) + g_i\left(V_i - V_{ref}^{Sec}\right) & \text{(30a)} \\ e_{Ci} = \sum\limits_{j\in\mathcal{N}_i^{Sec}} a_{ij}\left({I_i}^{C,pu} - {I_j}^{C,pu}\right) + g_i\left({I_i}^{C,pu} - I_{ref}^{Sec,pu}\right) & \text{(30b)} \end{cases}$$

where $\mathcal{N}_i^{Sec}$ is the set of communication neighbors of MG i, $a_{ij} = 1$ if the modules i and j can communicate with each other through a communication link, $g_i = 1$ if MG i can receive the reference values about voltage and per-unit current which means $i \in \mathcal{N}_L^{Sec}$, and $\mathcal{N}_L^{Sec}$ is the set for MGs who can receive the reference values.

The cascade of the above equations and the PI controllers are shown in the right part of Fig. 3 To be specific, the current reference value $I_{ref}^{Sec,pu}$ is a per-unit value considering the total load requirement and the total system capacity. If the per-unit values of all the output currents are equals to the reference, it means that MGs share the loads properly according to their own capacities.

In matrix form, (30) is given by the equations:

$$\begin{cases} e_V = (L+G)(V - V_{ref}^{Sec}\mathbf{1_N}) & \text{(31a)} \\ e_C = (L+G)(I_t^{C,pu} - I_{ref}^{Sec,pu}\mathbf{1_N}) & \text{(31b)} \end{cases}$$

where $e_V = [\ e_{V1}\ e_{V2}\ \dots\ e_{VN}]^T$, $V = [\ V_1\ V_2\ \dots\ V_N]^T$, $I_t^{C,pu} = [\ I_{t1}^{C,pu}\ I_{t2}^{C,pu}\ \dots\ I_{tn}^{C,pu}]^T$, and G is a diagonal matrix with diagonal entries equal to the gains g_i. Based on Assumption 2, L is symmetric Laplacian matrix.

Then, the error e_{Vi} and e_{Ci} are filtered by PI controllers respectively. The outputs ΔV_i and $\Delta I_{ti}^{C,pu}$ of the secondary controller layer can be written as

$$\begin{cases} \Delta V = -K_{pV}e_V - \int K_{iV}e_V & \text{(32a)} \\ \Delta I_t^{C,pu} = -K_{pC}e_C - \int K_{iC}e_C & \text{(32b)} \end{cases}$$

where $\Delta V = [\ \Delta V_1\ \Delta V_2\ \dots\ \Delta V_N]^T$, $\Delta I_t^{C,pu} = [\ \Delta I_{t1}^{C,pu}\ \Delta I_{t2}^{C,pu}\ \dots\ \Delta I_{tn}^{C,pu}]^T$. In addition, K_{pV} and K_{iV} are proportional and integral coefficients of the leader-based voltage controllers and K_{pC} and K_{iC} are proportional and integral coefficients of the leader-based current controllers. All the coefficients are common to all MGs, thus these are scalar variables.

The relationship between the primary PnP controller and the leader-based secondary controller are shown in the right block of Fig. 3. Exploiting the unit gain approximation of primary loops, one obtains that (29) is replaced by

$$\begin{cases} V = V_{ref}^{Pri} + \Delta V & \text{(33a)} \\ I_t^{C,pu} = I_{ref}^{Pri,pu} + \Delta I_t^{C,pu} & \text{(33b)} \end{cases}$$

where $V_{ref}^{Pri} = [\ V_{ref,1}^{Pri}\ V_{ref,2}^{Pri}\ \dots\ V_{ref,n}^{Pri}]^T$, $I_{ref}^{Pri,pu} = [\ I_{ref,1}^{Pri,pu}\ I_{ref,2}^{Pri,pu}\ \dots\ I_{ref,n}^{Pri,pu}]^T$.

Focusing on the time derivative of (33), we get

$$\begin{cases} \dot{V} = -K_{iV}[I + K_{pV}(L+G)]^{-1}e_V & \text{(34a)} \\ \dot{I}_t^{C,pu} = -K_{iC}[I + K_{pC}(L+G)]^{-1}e_C & \text{(34b)} \end{cases}$$

B. Stability Analysis

The aim is to show that under the effect of secondary control layer, all PCC voltage converge to the leader value V_{ref}^{Sec} and all the output current converge to the same per-unit value $I_{ref}^{Sec,pu}$. We start by introducing preliminary lemmas.

Lemma 3. *Under Assumption 2, L is symmetric Laplacian matrix. Since $G = diag[g_1, g_2, \dots, g_n] \geqslant 0$ is a diagonal matrix with at least one strictly positive entry, matrix $L+G$ is positive definite.*

Corollary 1. *Under the assumption of Lemma 3, for any scalar $\alpha > 0$, matrix $[I + \alpha(L+G)]^{-1}$ is positive definite.*

This article has been accepted for publication in a future issue of this journal, but has not been fully edited. Content may change prior to final publication. Citation information: DOI 10.1109/TPWRS.2018.2884876, IEEE Transactions on Power Systems

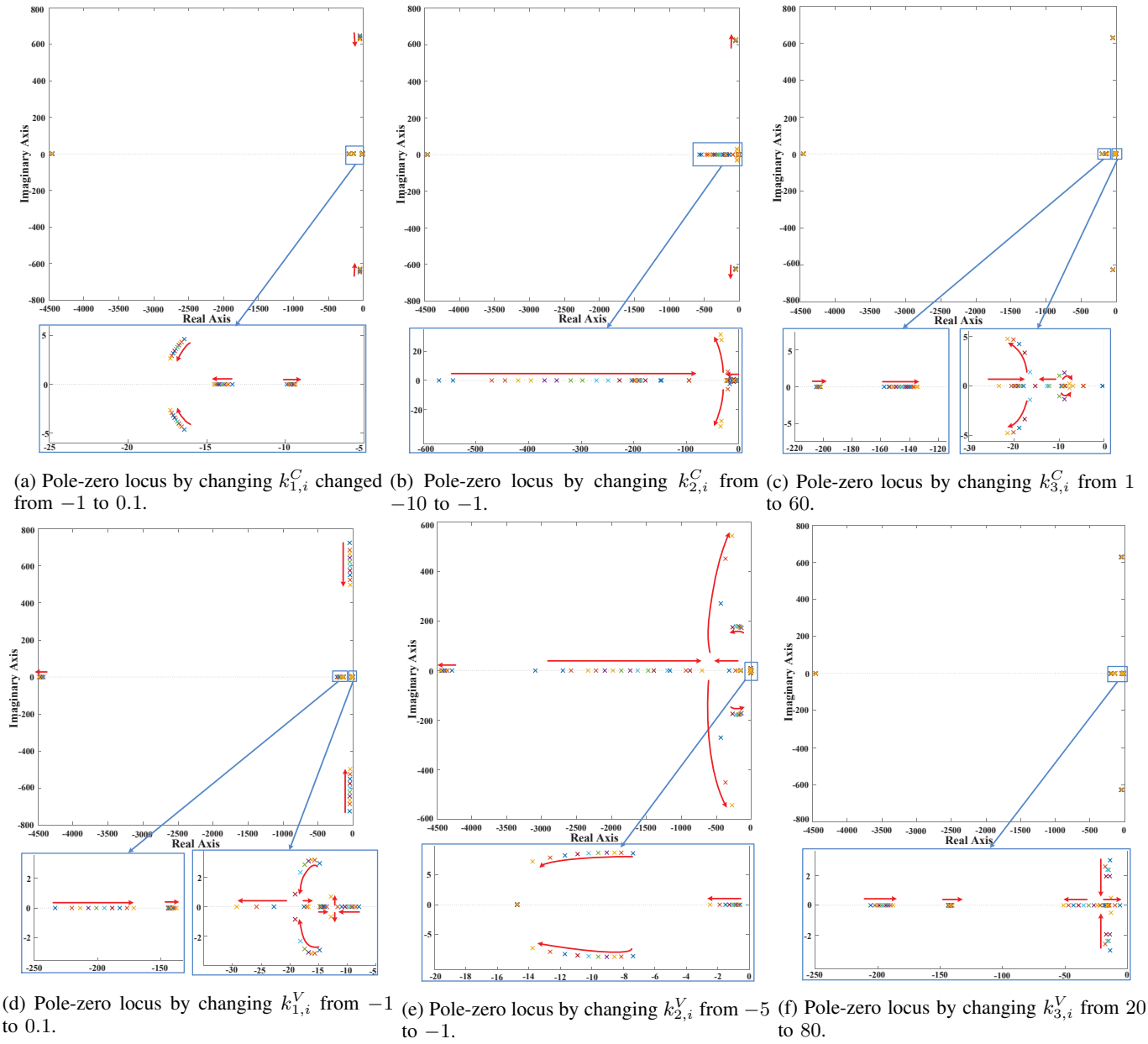

(a) Pole-zero locus by changing $k_{1,i}^C$ changed from -1 to 0.1.

(b) Pole-zero locus by changing $k_{2,i}^C$ from -10 to -1.

(c) Pole-zero locus by changing $k_{3,i}^C$ from 1 to 60.

(d) Pole-zero locus by changing $k_{1,i}^V$ from -1 to 0.1.

(e) Pole-zero locus by changing $k_{2,i}^V$ from -5 to -1.

(f) Pole-zero locus by changing $k_{3,i}^V$ from 20 to 80.

Fig. 5: Pole-zero locus analyses by changing control parameters.

Lemma 4. *[27] Let A, $B \in \mathbb{R}^{n\times n}$ be positive definite matrices. If $AB = BA$ is satisfied, then AB is positive definite.*

Lemma 5. *Under Lemma 4 and Corollary 1, for any scalar $K_{pV} > 0$, the matrix $(L+G)[I+K_{pV}(L+G)]^{-1}$ is positive definite.*

The proofs of Lemma 3, Corollary 1, and Lemma 5 are provided in the Appendix.

We are now in a position to introduce the theorem.

Theorem 2. *Based on Lemma 5, with the controller* (32)*, the tracking errors in* (31) *converge to zero.*

Proof. Note that the schemes (30a)-(32a) and (30b)-(32b) have the same structure. Then, in the following, we show convergence to the leader reference value only for voltages.

We consider the following candidate Lyapunov function

$$Z = \frac{1}{2} e_V^T P^{Sec} e_V, \text{ where } P^{Sec} > 0 \tag{35}$$

The time derivative of (35) is

$$\begin{aligned} \dot{Z} &= e_V^T P^{Sec}(L+G)\dot{V} \\ &= -K_{iV} e_V^T P^{Sec}(L+G)[I+K_{pV}(L+G)]^{-1} e_V \\ &= \frac{-K_{iV}}{2} e_V^T [P^{Sec}O + O^T P^{Sec}] e_V \end{aligned} \tag{36}$$

where $O = (L+G)[I+K_{pV}(L+G)]^{-1}$.

Based on Lemma 5, matrix O is positive definite. Based on Lyapunov theory [28], there exists positive definite matrix P^{Sec} which makes $P^{Sec}O + O^T P^{Sec}$ positive definite. (For such the linear time-invariant system $\dot{X} = -OX$, if the matrix

This article has been accepted for publication in a future issue of this journal, but has not been fully edited. Content may change prior to final publication. Citation information: DOI 10.1109/TPWRS.2018.2884876, IEEE Transactions on Power Systems

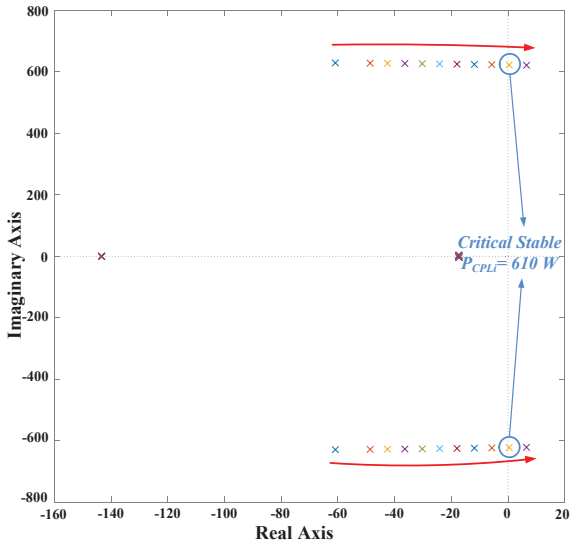

Fig. 6: Pole-zero locus by changing power of CPL from 0 W to 680 W for one MG.

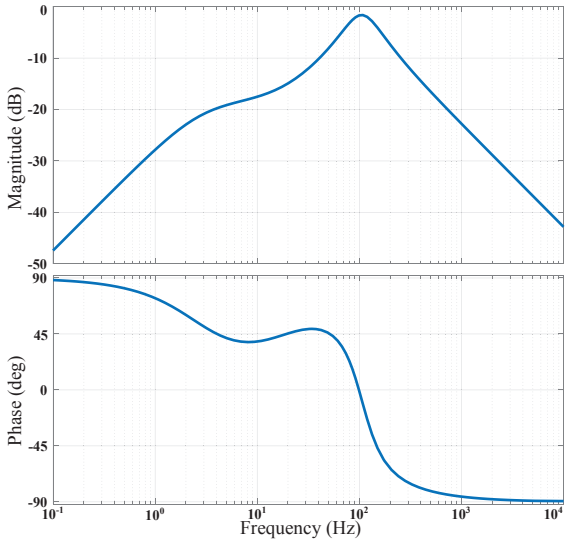

Fig. 7: Closed-loop system impedance profile.

O is positive definite, the system is asymptotically stable). Therefore

$$\begin{aligned}\dot{Z} =& \frac{-K_{iV}}{2} e_V^T [P^{Sec}O + O^T P^{Sec}] e_V \\ <& \frac{-K_{iV}}{2} \sigma_{min}(P^{Sec}O + O^T P^{Sec}) ||e_V||^2 < 0\end{aligned} \tag{37}$$

where $\sigma_{min}(P^{Sec}O + O^T P^{Sec})$ denotes the minimal eigenvalues of the symmetric matrix $P^{Sec}O + O^T P^{Sec}$. From (37), one has that the tracking error e_V goes to zero, and that all PCC voltages converge to the reference value provided by the leader. The convergence of output currents to the reference value can be shown in the same way. □

VI. Hardware-in-Loop Test

In order to verify the correctness of theoretical results, real-time HiL tests are carried out using dSPACE 1006 platform.

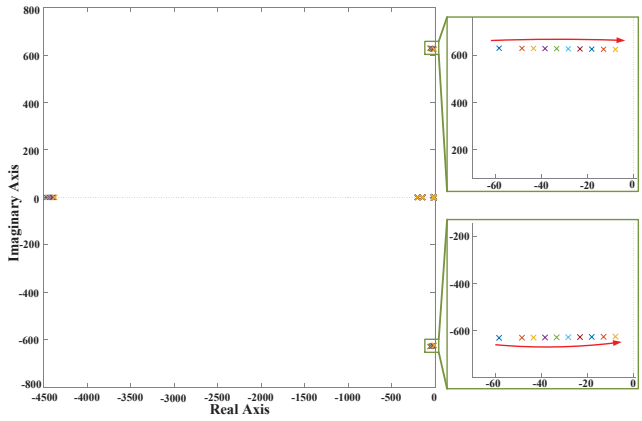

Fig. 8: Pole-zero locus by changing power of CPL from 0 W to 1000 W for a MG cluster.

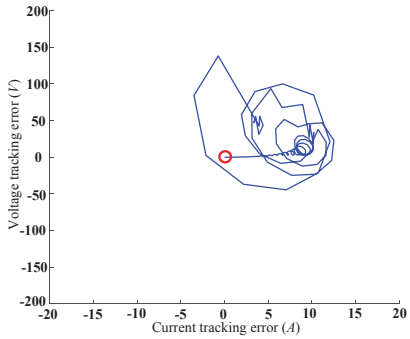

Fig. 9: Voltage/current tracking errors trajectory with $-1V$ initial voltage.

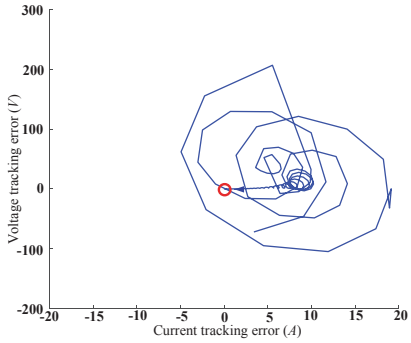

Fig. 10: Voltage/current tracking errors trajectory with $120V$ initial voltage.

The real-time test model comprises four MGs with meshed electrical topology shown in Fig. 11. The communication network is shown by the orange lines in the same figure. Moreover, MG 1 is the only MG receiving the leader information from energy management system (EMS). In each sampling period, each MG only communicate with their neighbors which means that the communication network is distributed. Since the communication topology is connected, the leader information can reach each follower in the system indirectly. The nominal voltage for the MG clusters is 48V. The electrical setup information are shown in Table I. The control parameters

This article has been accepted for publication in a future issue of this journal, but has not been fully edited. Content may change prior to final publication. Citation information: DOI 10.1109/TPWRS.2018.2884876, IEEE Transactions on Power Systems

are shown in Table II.

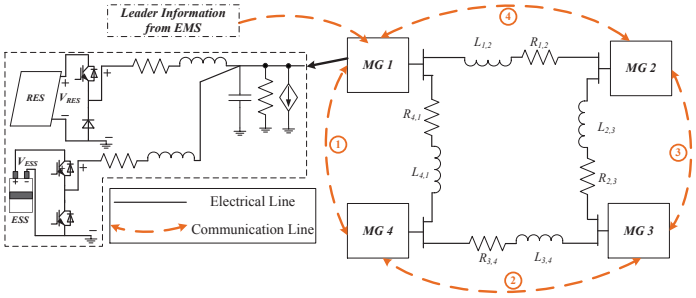

Fig. 11: System configuration of Hardware-in-Loop test.

TABLE I: Electrical setup parameters

Parameter	Symbol	Value
Output capacitance	C_{t*}	2.2 mF
Inductance for RES	L^C_{t*}	0.018 H
Inductor + switch loss resistance for RES	R^C_{t*}	0.2 Ω
Inductance for ESS	L^V_{t*}	0.0018 H
Inductor + switch loss resistance for ESS	R^V_{t*}	0.1 Ω
Switching frequency	f_{sw}	10 kHz

TABLE II: Control Parameters

Control Parameters	Symbol	Value
Primary Control Level for Single MG	$k^C_{1,*}$	-0.01
	$k^C_{2,*}$	-2.7015
	$k^C_{3,*}$	40.4018
	$k^V_{1,*}$	-0.480
	$k^V_{2,*}$	-0.108
	$k^V_{3,*}$	30.673
Secondary Control Level for MG Cluster	k_{pV}	4
	k_{iV}	22
	k_{pC}	3
	k_{iC}	20

A. Case 1: Instability Test

From (21), according to the system information reported above, the controller coefficient must verify

$$\begin{cases} k^C_{1,i} < 1 \\ k^C_{2,i} < 0.2 \\ k^C_{3,i} > 0 \end{cases}, \quad \begin{cases} k^V_{1,i} < 1 \\ k^V_{2,i} < 0.1 \\ 0 < k^V_{3,i} < \dfrac{1}{L^V_{ti}}(k^V_{1,i} - 1)(k^V_{2,i} - R^V_{ti}) \end{cases} \tag{38}$$

At the beginning, MGs are operated separately and at $t = 0.5s$ MGs are connected together to form the MG cluster. Then at $t = 1s$,, the control coefficients are changed in order to violate (38). Fig. 12 including six sub-figures illustrates the system performance when each control coefficient is changed from the stable region to the instable region. Fig. 12a to 12c show that when control coefficients for the grid-forming converter in MG 2 go sightly out of the stable region, the system becomes unstable. Fig. 12d to 12f show that the same happens when control coefficients for the grid-feeding converter in MG 2 slightly violate the inequalities. The results show that the control parameter set (21) can be tight for specific MG clusters.

B. Case 2: Voltage/Current Tracking Test

Voltage/current offset-free tracking is verified considering both the primary and secondary control level. At the beginning, four MGs are operated separately, using different voltage/current references. The results are shown in Figs. 13 and 14. At $T1$, four MGs are connected together simultaneously. As shown in Fig. 13a, apart from small oscillations on PCC voltages, the system operation is stable. Moreover, the output currents track the local reference provided by primary controllers as shown in Fig. 14. At $T2$, the proposed leader-based voltage controller is enabled and the leader value is set as $48V$. It is illustrated in Fig. 13a that after $T2$, the PCC voltages converge to the leader reference under $0.3s$. Then, at $T3$, the proposed leader-based current controller is enabled and leader value is set as $0.3p.u.$ Fig. 14 illustrates that the per-unit current values can converge to the leader value within $1s$. In addition, Fig. 13b illustrates that only $0.04V$ oscillations exist in the output voltages when enabling the leader-based current controller. Furthermore, when the reference for leader-based voltage controller is changed from $48V$ to $49V$ at $T4$, the PCC voltages still track the leader reference, as shown in Fig. 13a. Similarly, when the reference for leader-based current controller is changed from $0.3p.u.$ to $0.4p.u.$ at $T5$, the output currents can track the new value as shown in Fig. 14. Fig. 13c illustrates that when the reference for leader-based current is changed, the output voltages are not affected.

C. Case 3: PnP Function Test

The PnP function for both primary and secondary controllers is tested. At $T1$, four MGs are connected together simultaneously. At $T2$ and $T3$, the proposed leader-based voltage/current controllers are enabled, respectively. At $T4$, MG 2 is plugged out of the MG cluster, which means the communication links and electrical lines are all disconnected with the cluster. As shown in Figs. 15a and 15b, the other three MGs still operate in a stable way and then keep tracking the leader reference from the secondary control level. Meanwhile, MG 2 can still use its own primary controller following the reference from the primary control level which are $47.8V$ for voltage and $0.25p.u.$ for current. At $T5$, MG 2 is plugged into the cluster and the communication links of MG 2 are also enabled. As shown in Fig. 15a and 15b after $T5$, both the output voltage and current of MG 2 start to track the reference value of the leader node. Overall, the results show that even in presence of plug-in/out events, the MG cluster can behave in a stable way. And both output voltage and current tracking performance can be guaranteed. Furthermore, during the whole test, the control coefficients for all MGs are not changed.

D. Case 4: CPL Capacity Test

In accordance with the analysis condition in subsection IV-C, one MG with ZIP load is considered first. The power of CPL in the system is increased from 0 W to 600 W with 100

This article has been accepted for publication in a future issue of this journal, but has not been fully edited. Content may change prior to final publication. Citation information: DOI 10.1109/TPWRS.2018.2884876, IEEE Transactions on Power Systems

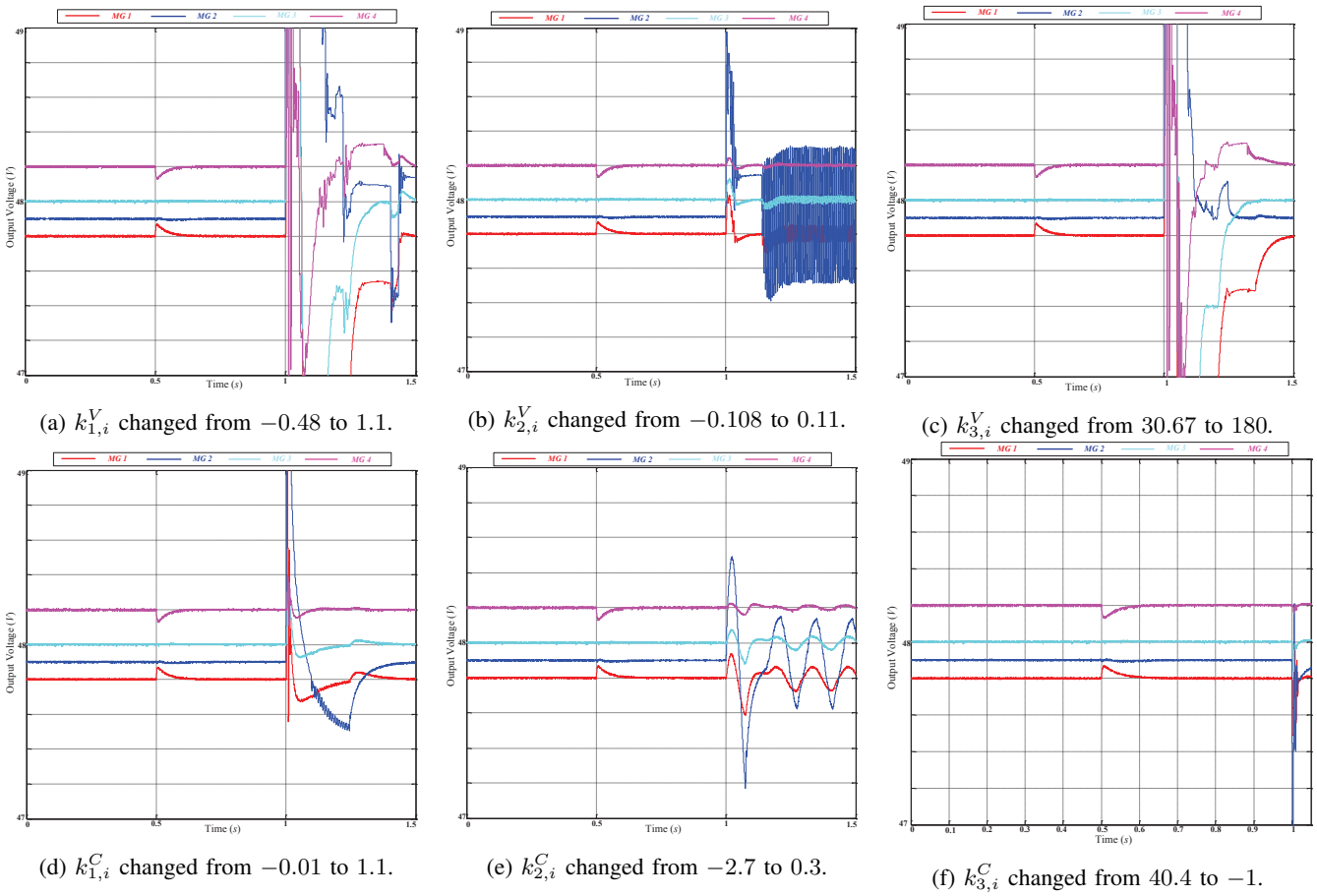

(a) $k_{1,i}^{V}$ changed from -0.48 to 1.1.

(b) $k_{2,i}^{V}$ changed from -0.108 to 0.11.

(c) $k_{3,i}^{V}$ changed from 30.67 to 180.

(d) $k_{1,i}^{C}$ changed from -0.01 to 1.1.

(e) $k_{2,i}^{C}$ changed from -2.7 to 0.3.

(f) $k_{3,i}^{C}$ changed from 40.4 to -1.

Fig. 12: Voltage profile of instability test for Case 1

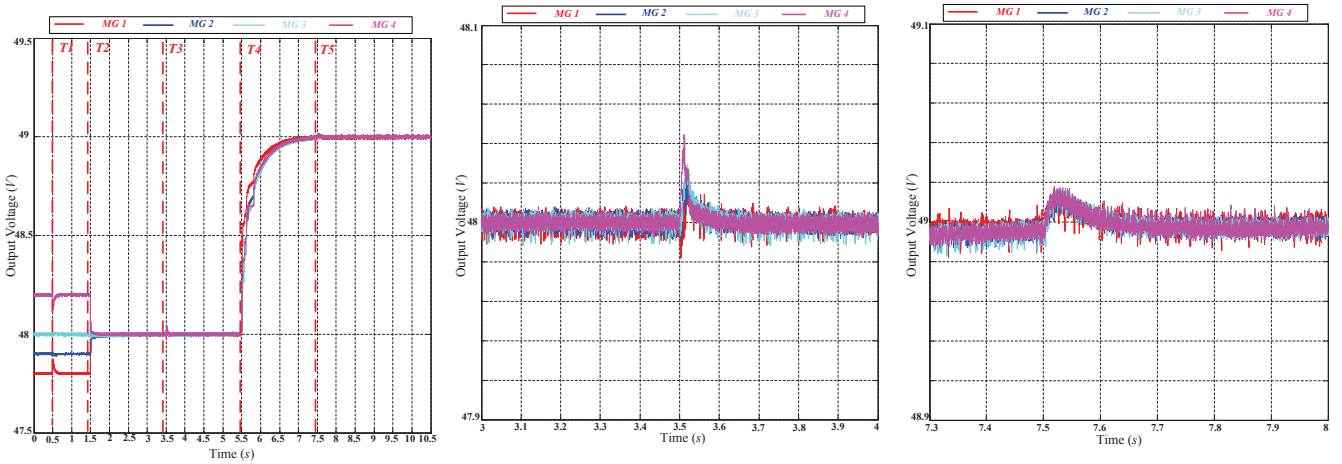

(a) Voltage performance.

(b) Zoomed in voltage performance between $3s$ and $4s$.

(c) Zoomed in voltage performance between $7.3s$ and $8s$.

Fig. 13: Voltage performance for voltage/current tracking test for Case 2.

W step. During the test, the current reference for RES is set at 5 A and the rest amount of power is absorbed or provided by ESS. The result are shown in Fig.16.

As shown in Fig.16a, the voltage can be stable for each CPL increasing step until the power of CPL reach 600 W. Meanwhile, during the same period, the current from RES shown in Fig. 16b is tracking its reference 5 A. The current performance from ESS is shown in Fig. 16c. At the beginning of the test, the current from RES is larger than the total load consumption, thus the current from ESS is negative which means it is charged. With the increasing power of CPL, the ESS start to provide the power into the system. When the system is subjected to the CPL power step from 500 W to 600 W, the system become unstable. The result is identical to

This article has been accepted for publication in a future issue of this journal, but has not been fully edited. Content may change prior to final publication. Citation information: DOI 10.1109/TPWRS.2018.2884876, IEEE Transactions on Power Systems

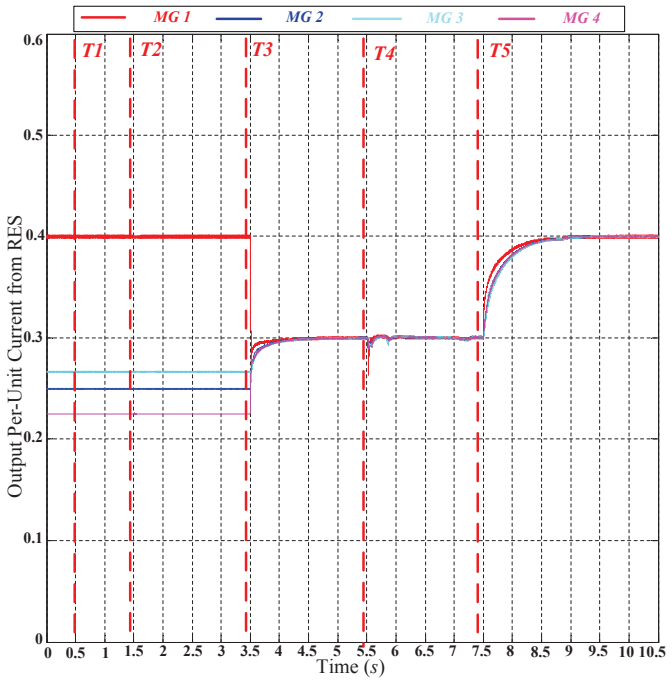

Fig. 14: Current performance for voltage/current tracking test for Case 2.

the analysis results shown in Fig. 6 which shows that when the CPL is increased to 600 W, a pair of pole appeared in the RHP make the system unstable.

Then a MG cluster consisting of MG 1 and MG 3 with ZIP loads is considered. The results are shown in Fig. 17. The power of CPL is increased from 0 W to 1100 W step by step during the whole test. Moreover, the different voltage references are set for two MGs: 48 V for MG 1 and 48.2 V for MG 3 to make the figure clear. The current references for two RESes are same and set at 5 A. During the whole test, the system can be kept stable. Compared with the test result with one MG, the CPL capacity of the MG cluster is more than twice larger than that of one MG. It means a new connected MG can provide more damping to the system. The analysis results in Fig. 8 also show that no pole goes into the RHP when the power of CPL reach 1000 W. And the accuracy of the analysis results is proven again.

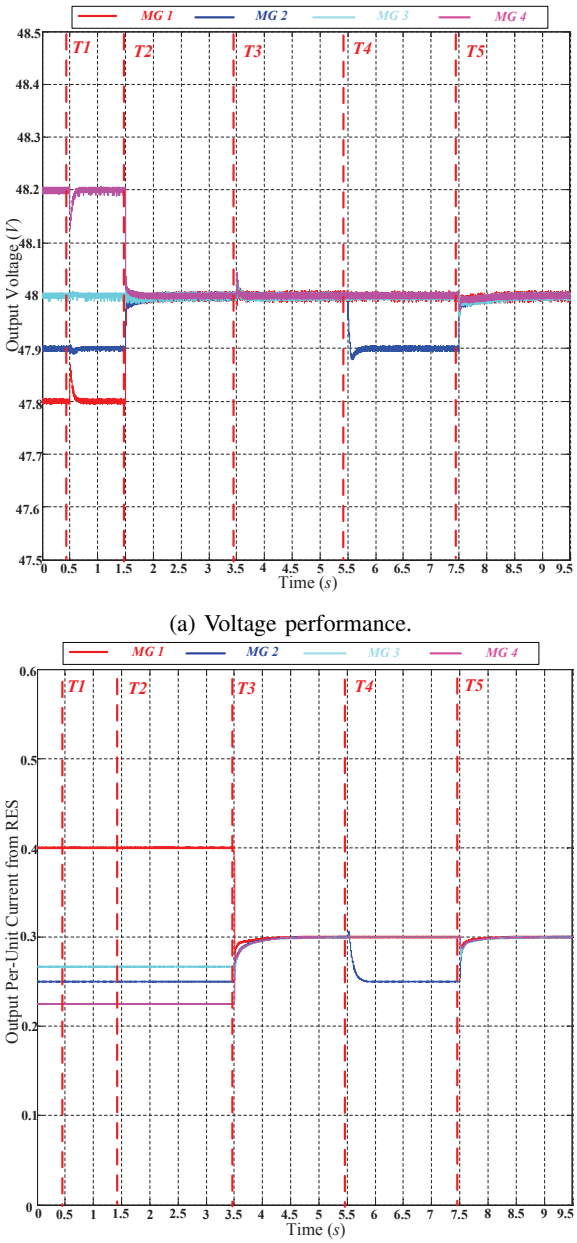

(a) Voltage performance.

(b) Current performance.

Fig. 15: Voltage and current performance for PnP test considering both the primary and secondary level for Case 3.

E. Case 5: Communication Delay Test

In this case, the effects of communication delays on the proposed secondary controller is studied.

Fig. 18 shows the system performance with 1000 μs communication delay. At t=$T1$, four MGs are connected together. At t=$T2$ and $T3$, the secondary voltage and current controllers are enabled respectively. At t=$T4$, $T5$, $T6$, and $T7$, 1000 μs communication delay is added in the communication links 1, 2, 3 and 4 respectively. It is shown that the voltage and current performance is not much deteriorated for delays up to 1000 μs.

Then, Fig. 19 shows the performance with 2000 μs delays. The start procedure is same as before. Then, at t=$T4$, $T5$, $T6$, and $T7$, the communication delay is added in the communication links 1, 2, 3 and 4 respectively. After adding delay for MG 4, oscillation around $\pm 0.5V$ exist in the output voltage in Fig. 19a, meanwhile small oscillation exist in the current in zoom in part of Fig. 19b. Even though oscillations exist in the system, it can still be operated stable under this condition. For counteracting the effect of delays, an option is to stop the secondary controller and keep the primary regulator only. To verify this operation, at t=$T8$, the secondary controller is disabled, after which, the oscillations disappear and both the voltage and current are stable operated.

This article has been accepted for publication in a future issue of this journal, but has not been fully edited. Content may change prior to final publication. Citation information: DOI 10.1109/TPWRS.2018.2884876, IEEE Transactions on Power Systems

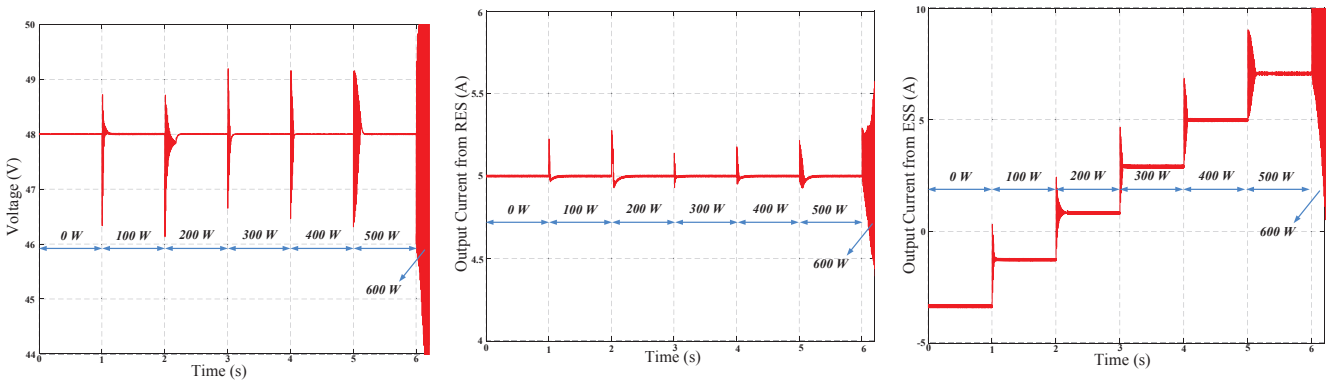

(a) Voltage performance.

(b) Current performance from grid-feeding converter.

(c) Current performance from grid-forming converter.

Fig. 16: Single MG performance under CPL change for Case 4.

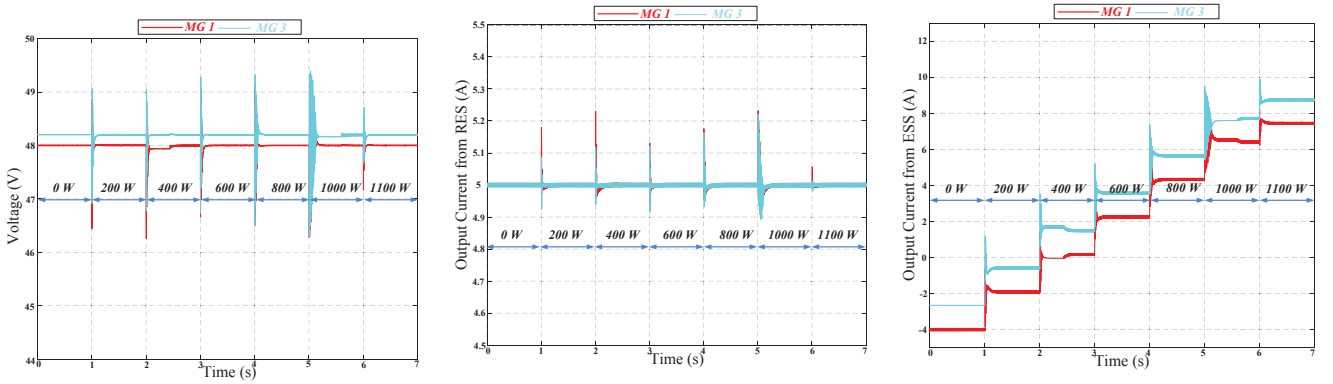

(a) Voltage performance.

(b) Current performance from grid-feeding converter.

(c) Current performance from grid-forming converter.

Fig. 17: MG cluster performance under CPL change for Case 4.

F. Case 6: Measurement Noise Test

The resilience to measurement noise is studied. Results are shown in Fig. 20 and 21. At t=$T1$, four MGs are connected together. At t=$T2$ and $T3$, the secondary voltage and current controllers are enabled respectively. At t=$T4$, the Gaussian white noise with 24 dB signal-noise-ratio (SNR) is added to each measured voltage and current. Notably, 24 dB SNR means the signal is quite poor according to the standard in [29]. It is shown in Fig. 20a and 21a that after t=$T4$, the noise is added in measured voltage and current which are used as control inputs for proposed controllers. The good performance of output voltage and current shown in 20b and 21b prove that the noise can be canceled by the controller and the performance cannot be affected under this poor measurement circumstance. In other words, the closed-loop system can performance as a low-pass filter to cancel the measurement noise to a certain degree.

VII. Conclusion

In this paper, a hierarchical PnP Voltage/Current controller for DC microgrid clusters with ZIP loads is proposed including primary control level and secondary control level. In the primary PnP controller, by choosing the control coefficients characterized by a set of inequalities which is only related to local parameters, the closed-loop stability can be guaranteed for the MG clusters. In the leader-based distributed secondary controller, both the voltage and current can track with the information from the higher control level by distributed communication strategy. Under the proposed hierarchical control structure, each MG can achieve plug-in/out operation without changing the control coefficients and knowing the electrical topology of MG clusters. As in [13], the proofs of closed-loop asymptotic stability of using the proposed controller for MG clusters exploit structured Lyapunov functions, the LaSalle invariance theorem and properties of graph Laplacians which shows that these tools offer a feasible theoretical framework for analyzing different kinds of MGs equipped with various types PnP decentralized control architectures. For more technical details, readers can refer to our original technical report [30].

References

[1] J. M. Guerrero, J. C. Vasquez, J. Matas, D. Vicuna, L. García, and M. Castilla, "Hierarchical control of droop-controlled AC and DC microgrids - A general approach toward standardization," *IEEE Transactions on Industrial Electronics*, vol. 58, no. 1, pp. 158–172, 2011.

This article has been accepted for publication in a future issue of this journal, but has not been fully edited. Content may change prior to final publication. Citation information: DOI 10.1109/TPWRS.2018.2884876, IEEE Transactions on Power Systems

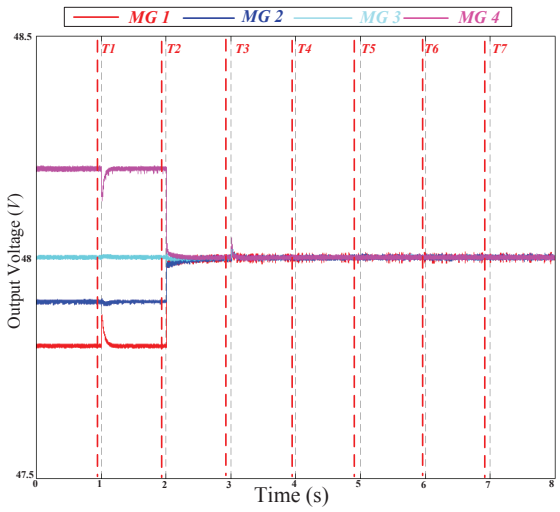

(a) Voltage performance.

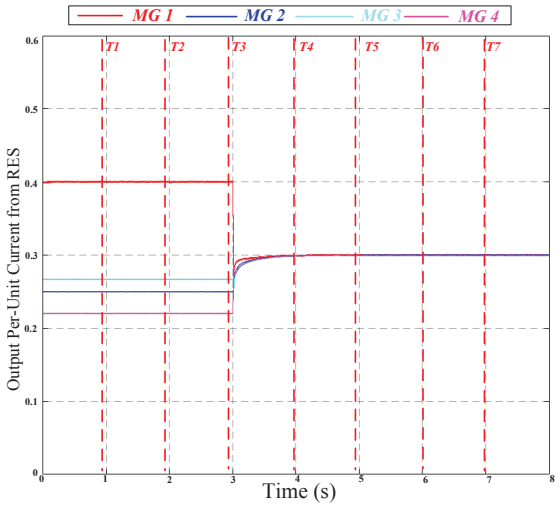

(b) Current performance.

Fig. 18: Control performance for 1000 μs communication delay test for Case 5.

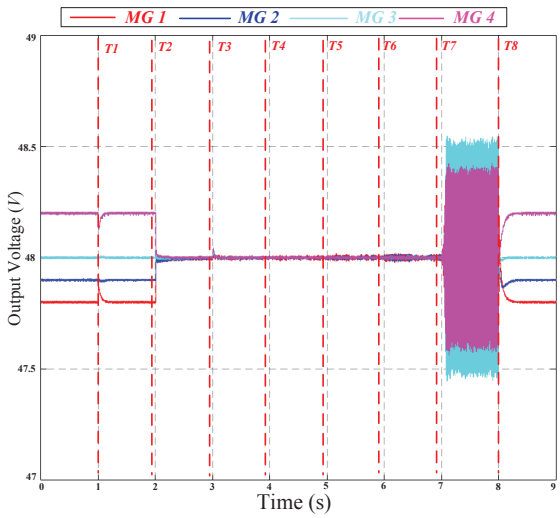

(a) Voltage performance.

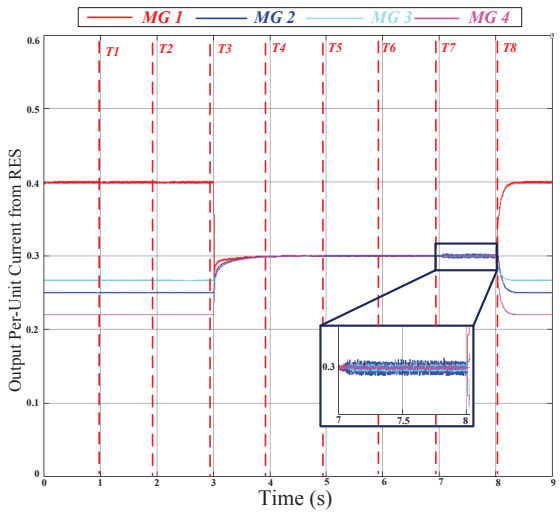

(b) Current performance.

Fig. 19: Control performance for 2000 μs communication delay test for Case 5.

[2] J. Schiffer, R. Ortega, A. Astolfi, J. Raisch, and T. Sezi, "Conditions for stability of droop-controlled inverter-based microgrids," *Automatica*, vol. 50, no. 10, pp. 2457 – 2469, 2014. [Online]. Available: http://www.sciencedirect.com/science/article/pii/S0005109814003100

[3] A. Iovine, M. J. Carrizosa, G. Damm, and P. Alou, "Nonlinear control for dc microgrids enabling efficient renewable power integration and ancillary services for ac grids," *IEEE Transactions on Power Systems*, pp. 1–1, 2018.

[4] J. Rocabert, A. Luna, F. Blaabjerg, and P. Rodríguez, "Control of power converters in ac microgrids," *IEEE Transactions on Power Electronics*, vol. 27, no. 11, pp. 4734–4749, Nov 2012.

[5] R. Han, L. Meng, G. Ferrari-Trecate, E. A. A. Coelho, J. C. Vasquez, and J. M. Guerrero, "Containment and consensus-based distributed coordination control to achieve bounded voltage and precise reactive power sharing in islanded ac microgrids," *IEEE Transactions on Industry Applications*, vol. 53, no. 6, pp. 5187–5199, Nov 2017.

[6] T. Dragičević, X. Lu, J. Vasquez, and J. Guerrero, "DC microgrids–part I: A review of control strategies and stabilization techniques," *IEEE Transactions on Power Electronics*, vol. 31, no. 7, pp. 4876–4891, 2016.

[7] J. Liu, W. Zhang, and G. Rizzoni, "Robust stability analysis of dc microgrids with constant power loads," *IEEE Transactions on Power Systems*, vol. 33, no. 1, pp. 851–860, Jan 2018.

[8] R. Han, L. Meng, J. M. Guerrero, and J. C. Vasquez, "Distributed nonlinear control with event-triggered communication to achieve current-sharing and voltage regulation in dc microgrids," *IEEE Transactions on Power Electronics*, vol. 33, no. 7, pp. 6416–6433, July 2018.

[9] Q. Shafiee, T. Dragičević, J. C. Vasquez, and J. M. Guerrero, "Hierarchical Control for Multiple DC-Microgrids Clusters," *IEEE Transactions on Energy Conversion*, vol. 29, no. 4, pp. 922–933, 2014.

[10] V. Nasirian, S. Moayedi, A. Davoudi, and F. L. Lewis, "Distributed cooperative control of dc microgrids," *IEEE Transactions on Power Electronics*, vol. 30, no. 4, pp. 2288–2303, April 2015.

[11] S. Riverso, M. Farina, and G. Ferrari-Trecate, "Plug-and-Play Model Predictive Control based on robust control invariant sets," *Automatica*, vol. 50, no. 8, pp. 2179–2186, 2014.

[12] M. Tucci, S. Riverso, J. C. Vasquez, J. M. Guerrero, and G. Ferrari-Trecate, "A decentralized scalable approach to voltage control of dc islanded microgrids," *IEEE Transactions on Control Systems Technology*, vol. 24, no. 6, pp. 1965–1979, Nov 2016.

[13] M. Tucci, S. Riverso, and G. Ferrari-Trecate, "Line-independent plug-and-play controllers for voltage stabilization in dc microgrids," *IEEE Transactions on Control Systems Technology*, vol. PP, no. 99, pp. 1–9, 2017.

[14] M. S. Sadabadi, Q. Shafiee, and A. Karimi, "Plug-and-play robust voltage control of dc microgrids," *IEEE Transactions on Smart Grid*, vol. PP, no. 99, pp. 1–1, 2017.

[15] C. Kim, Y. Gui, and C. C. Chung, "Maximum power point tracking of a wind power plant with predictive gradient ascent method," *IEEE*

This article has been accepted for publication in a future issue of this journal, but has not been fully edited. Content may change prior to final publication. Citation information: DOI 10.1109/TPWRS.2018.2884876, IEEE Transactions on Power Systems

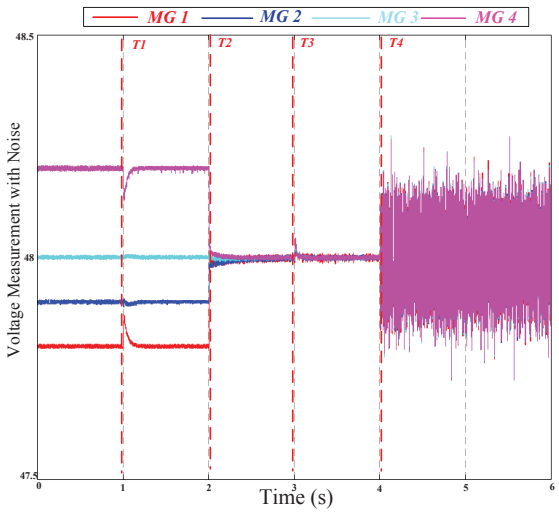

(a) Measured voltage with added noise.

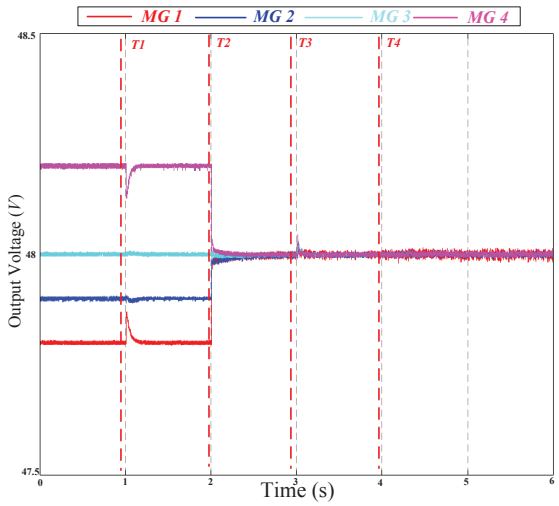

(b) Output voltage performance.

Fig. 20: Voltage for noise test for Case 6.

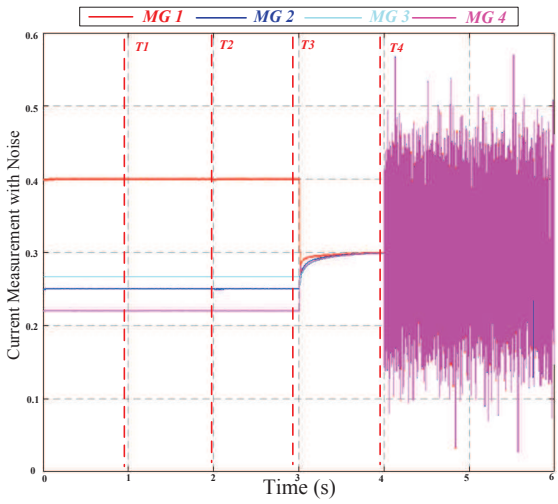

(a) Measured current with added noise.

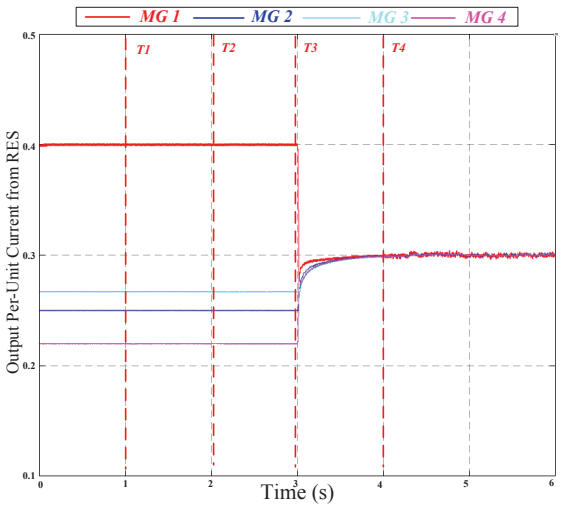

(b) Output current performance.

Fig. 21: Current performance for noise test for Case 6.

Transactions on Sustainable Energy, vol. 8, no. 2, pp. 685–694, April 2017.

[16] R. Han, M. Tucci, R. Soloperto, J. M. Guerrero, and G. Ferrari-Trecate, "Plug-and-play design of current controllers for grid-feeding converters in dc microgrids," in *2017 11th Asian Control Conference (ASCC)*, Dec 2017, pp. 2182–2187.

[17] J. Zhao and F. Dörfler, "Distributed control and optimization in DC microgrids," *Automatica*, vol. 61, pp. 18–26, 2015.

[18] D. Wu, F. Tang, T. Dragicevic, J. M. Guerrero, and J. C. Vasquez, "Coordinated control based on bus-signaling and virtual inertia for islanded dc microgrids," *IEEE Transactions on Smart Grid*, vol. 6, no. 6, pp. 2627–2638, Nov 2015.

[19] T. Dragicevic, J. M. Guerrero, J. C. Vasquez, and D. Skrlec, "Supervisory control of an adaptive-droop regulated DC microgrid with battery management capability," *IEEE Transactions on Power Electronics*, vol. 29, no. 2, pp. 695–706, Feb 2014.

[20] S. Sahoo and S. Mishra, "A distributed finite-time secondary average voltage regulation and current sharing controller for dc microgrids," *IEEE Transactions on Smart Grid*, pp. 1–1, 2018.

[21] R. Han, H. Wang, Z. Jin, L. Meng, and J. M. Guerrero, "Compromised controller design for current sharing and voltage regulation in dc microgrid," *IEEE Transactions on Power Electronics*, pp. 1–1, 2018.

[22] M. Tucci, L. Meng, J. M. Guerrero, and G. Ferrari-Trecate, "Consensus algorithms and plug-and-play control for current sharing in DC microgrids," *CoRR*, vol. abs/1603.03624, 2016. [Online]. Available: http://arxiv.org/abs/1603.03624

[23] S. Skogestad and I. Postlethwaite, *Multivariable feedback control: analysis and design*. New York, NY, USA: John Wiley & Sons, 1996.

[24] R. Middlebrook, "Input filter considerations in design and application of switching regulators," in *1976 IEEE Industrial Applications Society Annual Meeting*, March 1976, pp. 366–382.

[25] J. Liu, X. Feng, F. C. Lee, and D. Borojevich, "Stability margin monitoring for dc distributed power systems via perturbation approaches," *IEEE Transactions on Power Electronics*, vol. 18, no. 6, pp. 1254–1261, Nov 2003.

[26] F. Liu, J. Liu, H. Zhang, and D. Xue, "Stability issues of $z + z$ type cascade system in hybrid energy storage system (hess)," *IEEE Transactions on Power Electronics*, vol. 29, no. 11, pp. 5846–5859, Nov 2014.

[27] R. A. Horn and C. R. Johnson, *Matrix analysis*. Cambridge university press, 2012.

[28] Z. Qu, "Cooperative control of dynamical systems: applications to autonomous vehicles," 2009.

[29] P. Crilly and A. Carlson, *Communication Systems*. McGraw-Hill Education, 2009. [Online]. Available: https://books.google.dk/books?id=-hRGAQAAIAAJ

[30] R. Han, M. Tucci, R. Soloperto, A. Martinelli, G. Ferrari-Trecate, and J. M. Guerrero, "Hierarchical Plug-and-Play Voltage/Current Controller of DC microgrid Clusters with Grid-Forming/Feeding Converters: Line-independent Primary Stabilization and Leader-based Distributed Secondary Regulation," *ArXiv e-prints*, Jul. 2017.

[31] R. Grone, R. Merris, and V. S. Sunder, "The Laplacian spectrum of

a graph," *SIAM Journal on Matrix Analysis and Applications*, vol. 11, no. 2, pp. 218–238, 1990.
[32] C. Godsil and G. Royle, "Algebraic graph theory, volume 207 of graduate texts in mathematics," 2001.
[33] H. K. Khalil, *Nonlinear systems (3rd edition)*. Prentice Hall, 2001.
[34] N. Higham, *Accuracy and Stability of Numerical Algorithms*, 2nd ed. Society for Industrial and Applied Mathematics, 2002. [Online]. Available: http://epubs.siam.org/doi/abs/10.1137/1.9780898718027

Renke Han (S'16-M'18) was born in Liaoning, China, in 1991. He received the B.S. degree in Automation, the M.S. degree in Control Theory and Control Engineering both from Northeastern University, Shenyang, Liaoning Province, China, in 2013 and 2015 respectively, and Ph.D. degree in Power Electronics Systems from Aalborg University, Aalborg, Denmark, in 2018.

In 2017, he was as a Visiting Scholar with Laboratoire d'Automatique, École Polytechnique Fédérale de Lausanne (EPFL), Lausanne, Switzerland. Since November 2018, he joins Energy and Power Group, University of Oxford, UK, as a postdoctoral researcher. His research interests include high reliable and power density multi-port converter design, distributed controller for AC and DC microgrid.

He received an outstanding presentation award in Annual Conference of the IEEE Industrial Electronics Society, Italy in 2016 and the Outstanding Master Degree Thesis Award from Liaoning Province, China, in 2014.

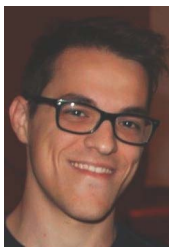

Michele Tucci (S'15-M'18) received the B.Sc. degree in electronic and telecommunications engineering, the M.Sc. degree in computer engineering and the Ph.D. degree in electronic, computer, and electrical engineering from the Università degli Studi di Pavia, Pavia, Italy, in 2012, 2014 and 2018, respectively.

He was a Master's Student with the ABB Corporate Research Center, Baden, Switzerland, in 2014, under the supervision of Dr. J. Poland. In 2014 and 2017, he was also a Visiting Ph.D. Student with the Microgrids Group, Aalborg University, Aalborg, Denmark, under the supervision of Prof. J. M. Guerrero, Prof. J. C. Vasquez and Dott. Lexuan Meng. His research interests includes distributed and scalable control applied to microgrids.

Andrea Martinelli joined the Automatic Control Laboratory of ETH Zürich in September 2018 as a Ph.D. student. He received the B.Sc. degree in Management and Production Engineering in 2015 and the M.Sc. degree in Automation and Control Engineering in 2017 cum laude, both from Politecnico di Milano, Italy. In 2017, he has been a visiting student at the Automatic Control Laboratory of EPFL, Lausanne, Switzerland, where he developed his M.Sc. thesis. In 2018, he has been a Research Assistant with the Systems & Control group at the Department of Electronics, Information and Bioengineering at Politecnico di Milano, Italy.

His research interests focus on the analysis and control of cyber-physical systems, with applications to microgrids. He has been exploring stabilizing techniques including distributed control, graph theory and passivity theory, as well as higher-layer architectures with the scope to coordinate the global network behavior.

Josep M. Guerrero (S'01-M'04-SM'08-FM'15) received the B.S. degree in telecommunications engineering, the M.S. degree in electronics engineering, and the Ph.D. degree in power electronics from the Technical University of Catalonia, Barcelona, in 1997, 2000 and 2003, respectively. Since 2011, he has been a Full Professor with the Department of Energy Technology, Aalborg University, Denmark, where he is responsible for the Microgrid Research Program (www.microgrids.et.aau.dk). From 2012 he is a guest Professor at the Chinese Academy of Science and the Nanjing University of Aeronautics and Astronautics; from 2014 he is chair Professor in Shandong University; from 2015 he is a distinguished guest Professor in Hunan University; and from 2016 he is a visiting professor fellow at Aston University, UK, and a guest Professor at the Nanjing University of Posts and Telecommunications.

His research interests are oriented to different microgrid aspects, including power electronics, distributed energy-storage systems, hierarchical and cooperative control, energy management systems, smart metering and the internet of things for AC/DC microgrid clusters and islanded minigrids; recently specially focused on maritime microgrids for electrical ships, vessels, ferries and seaports. Prof. Guerrero is an Associate Editor for the IEEE TRANSACTIONS ON POWER ELECTRONICS, He received the best paper award of the IEEE Transactions on Energy Conversion for the period 2014-2015, and the best paper prize of IEEE-PES in 2015. As well, he received the best paper award of the Journal of Power Electronics in 2016. In 2014, 2015, and 2016 he was awarded by Thomson Reuters as Highly Cited Researcher, and in 2015 he was elevated as IEEE Fellow for his contributions on "distributed power systems and microgrids."

Giancarlo Ferrari-Trecate (SM'12) received the Ph.D. degree in Electronic and Computer Engineering from the Universita' degli Studi di Pavia in 1999. Since September 2016 he is Professor at EPFL, Lausanne, Switzerland. In spring 1998, he was a Visiting Researcher at the Neural Computing Research Group, University of Birmingham, UK. In fall 1998, he joined as a Postdoctoral Fellow the Automatic Control Laboratory, ETH, Zurich, Switzerland. He was appointed Oberassistent at ETH, in 2000. In 2002, he joined INRIA, Rocquencourt, France, as a Research Fellow. From March to October 2005, he worked at the Politecnico di Milano, Italy. From 2005 to August 2016, he was Associate Professor at the Dipartimento di Ingegneria Industriale e dell'Informazione of the Universita' degli Studi di Pavia.

His research interests include scalable control design, networked state estimation, plug-and-play control of microgrids, modelling and analysis of biochemical networks, hybrid systems and Bayesian learning. Prof. Ferrari-Trecate was a recipient of the "assegno di ricerca" grant from the University of Pavia in 1999 and the Researcher Mobility Grant from the Italian Ministry of Education, University and Research in 2005. He is currently a member of the IFAC Technical Committees on Control Design and Optimal Control and he is on the editorial board of Automatica and Nonlinear Analysis: Hybrid Systems.

This article has been accepted for publication in a future issue of this journal, but has not been fully edited. Content may change prior to final publication. Citation information: DOI 10.1109/TPWRS.2018.2884876, IEEE Transactions on Power Systems

APPENDIX

A. Proof of Lemma 1

Proof. If $Q_i \leq 0$ is satisfied, from Proposition 1, the first block-row and block-column in (17) are null. Then $x^T Q_i x \leq 0$, $\forall x \in \mathbb{R}^5$. Partitioning x as

$$x = \begin{bmatrix} x_{11} \\ \tilde{x}_2 \\ \tilde{x}_4 \end{bmatrix}$$

where $\tilde{x}_{11} \in \mathbb{R}$, $\tilde{x}_2 \in \mathbb{R}^2$, $\tilde{x}_4 \in \mathbb{R}^2$.
We obtain

$$x^T Q_i x = \tilde{x}_2^T \mathcal{Q}_{22,i}^C \tilde{x}_2 + \tilde{x}_4^T \mathcal{Q}_{44,i}^V \tilde{x}_4.$$

For $\tilde{x}_2 = 0$ and $\tilde{x}_4 \neq 0$, one has

$$x^T Q_i x = \tilde{x}_4^T \mathcal{Q}_{44,i}^V \tilde{x}_4 \leq 0, \ \forall \tilde{x}_4 \in \mathbb{R}^2$$

which means

$$\mathcal{Q}_{44,i}^V \leq 0$$

Setting $\tilde{x}_4 = 0$ and $\tilde{x}_2 \neq 0$, one has

$$x^T Q_i x = \tilde{x}_2^T \mathcal{Q}_{22,i}^C \tilde{x}_2 \leq 0, \ \forall \tilde{x}_2 \in \mathbb{R}^2$$

which means

$$\mathcal{Q}_{22,i}^C \leq 0$$

□

B. Proof of Proposition 2

Proof. Based on (11) and (14), the upper middle block of (16) $\mathcal{Q}_{12,i}^C$ can be written as

$$[\mathcal{F}_{21,i}^C]^T \mathcal{P}_{22,i}^C + \eta_i \mathcal{F}_{12,i}^C = \left[\begin{array}{c|c} \frac{(k_{1,i}^C - 1)}{L_{ti}^C} p_{22,i}^C + \frac{1}{C_{ti}} \eta_i & \frac{(k_{1,i}^C - 1)}{L_{ti}^C} p_{23,i}^C \end{array} \right] \quad (39)$$

From Proposition 1, $\mathcal{Q}_{12,i}^C$ should be equal to zero vector which means

$$\begin{cases} \frac{(k_{1,i}^C - 1)}{L_{ti}^C} p_{22,i}^C = -\frac{1}{C_{ti}} \eta_i & (40a) \\ \frac{(k_{1,i}^C - 1)}{L_{ti}^C} p_{23,i}^C = 0 & (40b) \end{cases}$$

Because η_i is positive, thus it derives that

$$\begin{cases} k_{1,i}^C < 1 & (41a) \\ p_{23,i}^C = 0 & (41b) \end{cases}$$

With the results (41), the diagonal item of (16) $\mathcal{Q}_{22,i}^C$ can be direct recalculated as

$$[\mathcal{F}_{22,i}^C]^T \mathcal{P}_{22,i}^C + \mathcal{P}_{22,i}^C \mathcal{F}_{22,i}^C = \left[\begin{array}{c|c} 2\frac{(k_{2,i}^C - R_{ti}^C)}{L_{ti}^C} p_{22,i}^C & -p_{33,i}^C + \frac{k_{3,i}^C}{L_{ti}^C} p_{22,i}^C \\ \hline -p_{33,i}^C + \frac{k_{3,i}^C}{L_{ti}^C} p_{22,i}^C & 0 \end{array} \right] \quad (42)$$

Again from Proposition 1, the off diagonal item of (42) should be equal to zero which means

$$\frac{k_{3,i}^C}{L_{ti}^C} p_{22,i}^C = p_{33,i}^C \quad (43)$$

Thus,based on (43) and $P_i > 0$

$$k_{3,i}^C > 0 \quad (44)$$

From Proposition 1, Q_i should be at least negative semidefinite, thus

$$k_{2,i}^C < R_{ti}^C \quad (45)$$

Because the upper left corner 3×3 matrix of P_i is diagonal matrix and the matrix P_i is positive definite, one has

$$p_{44,i}^V > 0 \quad (46)$$

Based on (11) and (14), the off diagonal of (16) $\mathcal{Q}_{14,i}^V$ can be written as

$$[\mathcal{F}_{41,i}^V]^T \mathcal{P}_{44,i}^V + \eta_i \mathcal{F}_{14,i}^V = \left[\begin{array}{c|c} \frac{(k_{1,i}^V - 1)}{L_{ti}^V} p_{44,i}^V - p_{45,i}^V + \frac{1}{C_{ti}} \eta_i & \frac{(k_{1,i}^V - 1)}{L_{ti}^V} p_{45,i}^V - p_{55,i}^V \end{array} \right] \quad (47)$$

From Proposition 1, $\mathcal{Q}_{14,i}^V$ is a zero vector which means

$$\begin{cases} p_{45,i}^V = \frac{(k_{1,i}^V - 1)}{L_{ti}^V} p_{44,i}^V + \frac{1}{C_{ti}} \eta_i & (48a) \\ p_{55,i}^V = \frac{(k_{1,i}^V - 1)}{L_{ti}^V} p_{45,i}^V & (48b) \end{cases}$$

Then by explicitly computation of $\mathcal{Q}_{44,i}^V$, we can derive that

$$[\mathcal{F}_{44,i}^V]^T \mathcal{P}_{44,i}^V + \mathcal{P}_{44,i}^V \mathcal{F}_{44,i}^V = \left[\begin{array}{c|c} 2\frac{(k_{2,i}^V - R_{ti}^V)}{L_{ti}^V} p_{44,i}^V & \frac{(k_{2,i}^V - R_{ti}^V)}{L_{ti}^V} p_{45,i}^V + \frac{k_{3,i}^V}{L_{ti}^V} p_{44,i}^V \\ \hline \frac{(k_{2,i}^V - R_{ti}^V)}{L_{ti}^V} p_{45,i}^V + \frac{k_{3,i}^V}{L_{ti}^V} p_{44,i}^V & 2\frac{k_{3,i}^V}{L_{ti}^V} p_{45,i}^V \end{array} \right] \quad (49)$$

Based on the Lemma 1 and eq. (46)

$$2\frac{(k_{2,i}^V - R_{ti}^V)}{L_{ti}^V} p_{44,i}^V \leq 0 \Longrightarrow k_{2,i}^V \leq R_{ti}^V \quad (50)$$

Computing the determinant of $\mathcal{Q}_{44,i}^V$, one obtains

$$det(\mathcal{Q}_{44,i}^V) = -\left[\frac{(k_{2,i}^V - R_{ti}^V)}{L_{ti}^V} p_{45,i}^V - \frac{k_{3,i}^V}{L_{ti}^V} p_{44,i}^V \right]^2 \quad (51)$$

Based on the Lemma 1, the second principal minor of $\mathcal{Q}_{44,i}^V$ which is also the determinant $\mathcal{Q}_{44,i}^V$ is nonnegative. From (51), the maximum value is zero, thus the determinant of $\mathcal{Q}_{44,i}^V$ should be equal to zero. It follows that

$$\frac{(k_{2,i}^V - R_{ti}^V)}{L_{ti}^V} p_{45,i}^V = \frac{k_{3,i}^V}{L_{ti}^V} p_{44,i}^V \Longrightarrow p_{44,i}^V = \frac{(k_{2,i}^V - R_{ti}^V)}{k_{3,i}^V} p_{45,i}^V \quad (52)$$

By solving the system of equation given by (48) and (52), it follows that

$$\begin{cases} p_{44,i}^V = \frac{L_{ti}^V}{C_{ti}^V} \frac{(k_2^V - R_{ti}^V)}{h_i} & (53a) \\ p_{45,i}^V = \frac{L_{ti}^V}{C_{ti}} \frac{k_{3,i}^V}{h_i} & (53b) \\ p_{55,i}^V = \frac{1}{C_{ti}} \frac{k_{3,i}^V (k_1^V - 1)}{h_i} & (53c) \end{cases}$$

This article has been accepted for publication in a future issue of this journal, but has not been fully edited. Content may change prior to final publication. Citation information: DOI 10.1109/TPWRS.2018.2884876, IEEE Transactions on Power Systems

where $h_i = L_{ti}^V k_3^V - (k_1^V - 1)(k_2^V - R_{ti}^V)$.

Because $P_{44,i}^V$ is positive definite, all its principal minor should be positive definite. Then

- $det\left(\frac{L_{ti}^V}{C_{ti}^V}\frac{(k_2^V - R_{ti}^V)}{h_i}\right) > 0$, combining this result with (50), the feasible parameters $k_{2,i}^V$ and h_i set should be $Z_1 = \{k_2^V < R_{ti}^V\} \cap \{h < 0\}$
- $det\left(\left[\begin{array}{c|c} \frac{L_{ti}^V}{C_{ti}^V}\frac{(k_2^V - R_{ti}^V)}{h_i} & \frac{L_{ti}^V}{C_{ti}}\frac{k_{3,i}^V}{h_i} \\ \hline \frac{L_{ti}^V}{C_{ti}}\frac{k_{3,i}^V}{h_i} & \frac{1}{C_{ti}}\frac{k_{3,i}^V(k_1^V-1)}{h_i} \end{array}\right]\right) = -\frac{L_{ti}^V K_3^V}{C_t^2 h_i} > 0$, considering this result, the feasible parameters $k_{3,i}^V$ and h_i set should be $Z_2 = \{\{k_3^V < 0\} \cap \{h > 0\}\} \cup \{\{k_3^V > 0\} \cap \{h < 0\}\}$

By combing the Z_1 and Z_2 together, one has

$$\boldsymbol{Z} = \{Z_1\} \cap \{Z_2\} = \{k_2^V < R_{ti}^V\} \cap \{k_3^V > 0\} \cap \{h < 0\} \quad (54)$$

Because $k_3^V > 0$, the set $\{h < 0\}$ can be further split. Then, combining the set with (54), it can derive that

$$\boldsymbol{Z} = \{k_1^V < 1\} \cap \{k_2^V < R_{ti}^V\} \cap \{0 < k_3^V < \frac{1}{L_{ti}^V}(k_1^V - 1)(k_2^V - R_{ti}^V)\} \quad (55)$$

Thus, (20) can be derived by combining the result in (41b), (43) and(53). Then, combining the results in (41a), (44), (45) and (55), the set for control coefficients (21) is derived. □

C. Proof of Proposition 3

Proof. In the sequel, the subscript i is omitted for convenience. From (20), $g(w)$ is equal to

$$\left[\begin{array}{c|c|c} w_1 & w_2^T & w_3^T \end{array}\right] \left[\begin{array}{c|c|c|c|c} 0 & 0 & 0 & 0 & 0 \\ \hline 0 & 2\frac{(k_2^C - R_t^C)}{L_t^C}p_{22}^C & 0 & 0 & 0 \\ 0 & 0 & 0 & 0 & 0 \\ \hline 0 & 0 & 0 & q_{44}^V & q_{45}^V \\ 0 & 0 & 0 & q_{45}^V & q_{55}^V \end{array}\right] \left[\begin{array}{c} w_1 \\ \hline w_2 \\ \hline w_3 \end{array}\right] \quad (56)$$

where $w_2, w_3 \in \mathbb{R}^2$. Since Q is negative semidefinite, the vectors $\bar{w}$ satisfying (22) also maximize $g(\cdot)$. Hence, it must hold $\frac{\mathrm{d}g}{\mathrm{d}w}(\bar{w}) = Q\bar{w} = 0$, i.e.

$$\left[\begin{array}{c|c|c|c|c} 0 & 0 & 0 & 0 & 0 \\ \hline 0 & 2\frac{(k_2^C - R_t^C)}{L_t^C}p_{22}^C & 0 & 0 & 0 \\ 0 & 0 & 0 & 0 & 0 \\ \hline 0 & 0 & 0 & q_{44}^V & q_{45}^V \\ 0 & 0 & 0 & q_{45}^V & q_{55}^V \end{array}\right] \left[\begin{array}{c} \bar{w}_1 \\ \hline \bar{w}_2 \\ \hline \bar{w}_3 \end{array}\right] = 0. \quad (57)$$

Based on the results in Proposition 2, it is easy to show that, by direct calculation, a set of solutions to (22) and (57) is composed of vectors in the form

$$\bar{w} = \left[\begin{array}{ccccc} \alpha & 0 & \gamma & 0 & 0 \end{array}\right]^T, \quad \alpha, \gamma \in \mathbb{R}. \quad (58)$$

Moreover, from (56), we have that (22) is also verified if there exist vectors

$$\tilde{w} = \left[\begin{array}{c|c|c} w_1 & w_2^T & \underline{w}_3^T \end{array}\right]^T, \quad \underline{w}_3 \neq [0\ 0]^T, \quad (59)$$

such that $w_1 \in \mathbb{R}$, $w_2 \in \mathbb{R}^2$and

$$\underline{w}_3^T Q_{44}^V \underline{w}_3 = 0. \quad (60)$$

By exploiting the result of Lemma 2, we know that vectors $\underline{w}_3$ fulfilling (60) belong to $\mathrm{Ker}(F_{44}^V)$, which, recalling (14), can be explicitly computed as follows

$$\begin{aligned} \mathrm{Ker}(\mathcal{F}_{44}^V) &= \left\{x \in \mathbb{R}^2 : \left[\begin{array}{cc} f_{44}^V & f_{45}^V \\ 0 & 0 \end{array}\right] x = 0\right\} = \\ &= \left\{x \in \mathbb{R}^2 : x = [\ \beta\ \delta\beta\ ]^T, \beta \in \mathbb{R}, \delta = -\frac{k_2^V - R_t^V}{k_3^V}\right\}. \end{aligned} \quad (61)$$

The proof ends by merging (58) and (59), with $\underline{w}_3$ as in (61). □

D. Proof of Proposition 4

Proof. Consider the following decomposition of matrix $\hat{\mathbf{A}}$

$$\hat{\mathbf{A}} = \hat{\mathbf{A}}_\mathbf{D} + \hat{\mathbf{A}}_\mathbf{\Xi} + \hat{\mathbf{A}}_\mathbf{L} + \hat{\mathbf{A}}_\mathbf{C}, \quad (62)$$

where $\hat{\mathbf{A}}_\mathbf{D} = \mathrm{diag}(\hat{A}_{ii}, \ldots, \hat{A}_{NN})$ collects the local dynamics only, $\hat{\mathbf{A}}_\mathbf{C}$ collects the coupling dynamic representing the off-diagonal items of matrix $\hat{\mathbf{A}}$. Meanwhile, $\hat{\mathbf{A}}_\mathbf{\Xi} = \mathrm{diag}(\hat{A}_{\xi 1}, \ldots, \hat{A}_{\xi N})$ and $\hat{\mathbf{A}}_\mathbf{L} = \mathrm{diag}(\hat{A}_{load,1}, \ldots, \hat{A}_{load,N})$ with

$$\hat{A}_{\xi i} = \left[\begin{array}{cc} -\sum_{j \in \mathcal{N}_i}\frac{1}{R_{ij}C_{ti}} & \mathbf{0}_{1\times 4} \\ \mathbf{0}_{4\times 1} & \mathbf{0}_{4\times 4} \end{array}\right], \hat{A}_{load,i} = \left[\begin{array}{cc} -\frac{1}{R_{Li}C_{ti}} & \mathbf{0}_{1\times 4} \\ \mathbf{0}_{4\times 1} & \mathbf{0}_{4\times 4} \end{array}\right].$$

takes into account the dependence of each local state on the neighboring MGs and the local resistive load. According to the decomposition (62), the inequality (26) is equivalent to show that

$$\underbrace{(\hat{\mathbf{A}}_\mathbf{D} + \hat{\mathbf{B}}\mathbf{K})^\mathbf{T}\mathbf{P} + \mathbf{P}(\hat{\mathbf{A}}_\mathbf{D} + \hat{\mathbf{B}}\mathbf{K})}_{(a)} + \underbrace{\mathbf{2}(\hat{\mathbf{A}}_\mathbf{\Xi} + \hat{\mathbf{A}}_\mathbf{L})\mathbf{P}}_{(b)} + \underbrace{\hat{\mathbf{A}}_\mathbf{C}^\mathbf{T}\mathbf{P} + \mathbf{P}\hat{\mathbf{A}}_\mathbf{C}}_{(c)} \leq 0 \quad (63)$$

By means of Proposition 1, matrix $(a) = \mathrm{diag}(Q_1, \ldots, Q_N)$ is negative semidefinite. Then, the contribution of $(b) + (c)$ in (63) is studied as follows. Matrix (b), by construction, is block diagonal and collects on its diagonal blocks in the form

$$\begin{aligned} &2(\hat{A}_{\xi i} + \hat{A}_{load,i}^C)P_i = \\ &= \left[\begin{array}{cc} -2\frac{1}{R_{Li}C_{ti}} - 2\sum_{j \in \mathcal{N}_i}\frac{1}{R_{ij}C_{ti}} & \mathbf{0}_{1\times 4} \\ \mathbf{0}_{4\times 1} & \mathbf{0}_{4\times 4} \end{array}\right] \left[\begin{array}{c|c|c} \eta_i & \mathbf{0}_{1\times 2} & \mathbf{0}_{1\times 2} \\ \hline \mathbf{0}_{2\times 1} & \mathcal{P}_{22,i}^C & \mathbf{0}_{2\times 2} \\ \hline \mathbf{0}_{2\times 1} & \mathbf{0}_{2\times 2} & \mathcal{P}_{44,i}^V \end{array}\right] \\ &= \left[\begin{array}{cc} -2\tilde{\eta}_i - 2\sum_{j \in \mathcal{N}_i}\tilde{\eta}_{ij} & \mathbf{0}_{1\times 4} \\ \mathbf{0}_{4\times 1} & \mathbf{0}_{4\times 4} \end{array}\right] \end{aligned} \quad (64)$$

where

$$\tilde{\eta}_{ij} = \frac{\eta_i}{R_{ij}C_{ti}}, \ \tilde{\eta}_{Li} = \frac{\eta_i}{R_{Li}C_{ti}} \quad (65)$$

Considering matrix (c), each the block in position (i, j) is equal to

$$\left\{\begin{array}{ll} (\hat{A}_{ji})^T P_j + P_i \hat{A}_{ij} & \text{if } j \in \mathcal{N}_i \\ 0 & \text{otherwise} \end{array}\right.$$

where

$$P_i\hat{A}_{ij} + \hat{A}_{ji}^T P_j = \left[\begin{array}{cc} \tilde{\eta}_{ij} + \tilde{\eta}_{ji} & \mathbf{0}_{1\times 4} \\ \mathbf{0}_{4\times 1} & \mathbf{0}_{4\times 4} \end{array}\right]. \quad (66)$$

From (64) and (66), we notice that only the elements in position $(1, 1)$ of each 5×5 block of $(b) + (c)$ can be different

This article has been accepted for publication in a future issue of this journal, but has not been fully edited. Content may change prior to final publication. Citation information: DOI 10.1109/TPWRS.2018.2884876, IEEE Transactions on Power Systems

$$\mathcal{L} = \begin{bmatrix} (-2\tilde{\eta}_1 - 2\sum_{j\in\mathcal{N}_1}\tilde{\eta}_{1j}) & \bar{\eta}_{12} & \cdots & \bar{\eta}_{1N} \\ \bar{\eta}_{21} & \ddots & \ddots & \vdots \\ \vdots & \ddots & (-2\tilde{\eta}_{N-1} - 2\sum_{j\in\mathcal{N}_{N-1}}\tilde{\eta}_{N-1j}) & \bar{\eta}_{N-1N} \\ \bar{\eta}_{N1} & \cdots & \bar{\eta}_{NN-1} & (-2\tilde{\eta}_N - 2\sum_{j\in\mathcal{N}_N}\tilde{\eta}_{Nj}) \end{bmatrix} \quad (67)$$

from zero. Hence, in order to evaluate the positive/negative definiteness of the $5N \times 5N$ matrix $(b) + (c)$, we can equivalently consider the $N \times N$ matrix as (67) obtained by deleting the second to fifth rows and columns in each block of $(b) + (c)$. One has $\mathcal{L} = \mathcal{M} + \mathcal{U} + \mathcal{G}$, where

$$\mathcal{M} = \begin{bmatrix} -2\sum_{j\in\mathcal{N}_1}\tilde{\eta}_{1j} & 0 & \cdots & 0 \\ 0 & -2\sum_{j\in\mathcal{N}_2}\tilde{\eta}_{2j} & \ddots & \vdots \\ \vdots & \ddots & \ddots & 0 \\ 0 & \cdots & 0 & -2\sum_{j\in\mathcal{N}_N}\tilde{\eta}_{Nj} \end{bmatrix},$$

$$\mathcal{U} = \begin{bmatrix} -2\tilde{\eta}_{L1} & 0 & \cdots & 0 \\ 0 & -2\tilde{\eta}_{L2} & \ddots & \vdots \\ \vdots & \ddots & \ddots & 0 \\ 0 & \cdots & 0 & -2\tilde{\eta}_{LN} \end{bmatrix}$$

and

$$\mathcal{G} = \begin{bmatrix} 0 & \bar{\eta}_{12} & \cdots & \bar{\eta}_{1N} \\ \bar{\eta}_{21} & 0 & \ddots & \vdots \\ \vdots & \ddots & \ddots & \bar{\eta}_{N-1N} \\ \bar{\eta}_{N1} & \cdots & \bar{\eta}_{NN-1} & 0 \end{bmatrix}. \quad (68)$$

Notice that each off-diagonal element $\bar{\eta}_{ij}$ of $\mathcal{G}$ in (68) is equal to

$$\bar{\eta}_{ij} = \begin{cases} (\tilde{\eta}_{ij} + \tilde{\eta}_{ji}) & \text{if } j \in \mathcal{N}_i \\ 0 & \text{otherwise} \end{cases} \quad (69)$$

At this point, from Assumption 1, one obtains that $\tilde{\eta}_{ij} = \tilde{\eta}_{ji}$ (see (65)) and, consequently, $\bar{\eta}_{ij} = \bar{\eta}_{ji} = 2\tilde{\eta}_{ij}$ (see (69)). Hence, $-(\mathcal{M} + \mathcal{G})$ is symmetric and has non negative off-diagonal elements which means it is a Laplacian matrix [31], [32] which is semi positive definite. Then, the properties of matrix $-\mathcal{U}$ should be considered. Since the negative impedance from CPL is considered, the definite property of $-\mathcal{U}$ depends on the each diagonal items $\tilde{\eta}_{Li}$ which is directly related to the equivalent resistance R_{Li} shown in eq. (2). To calculate in details as

$$\tilde{\eta}_{Li} = \frac{\eta_i}{C_{ti}}(\frac{1}{R_i} - \frac{P_{CPLi}}{V_{op}^2}). \quad (70)$$

For each diagonal item in matrix $\mathcal{U}$, since $\eta_i > 0$ and $C_{ti} > 0$, if the condition $P_{CPLi} \leq \frac{V_{op}^2}{R_i}$ is satisfied, then all the diagonal items satisfy $\tilde{\eta}_{Li} \geq 0$. It means matrix $-\mathcal{U}$ is a zero matrix under the worst condition or a positive-definite matrix under the best condition, further, the matrix $-\mathcal{U}$ is a semi-positive definite matrix between the two extreme conditions. It follows that $-\mathcal{L}$ is equals to a Laplacian matrix plus a zero matrix, or a semi-positive/positive definite diagonal matrix. As such, it verifies $\mathcal{L} \leq 0$ by construction. By adding the deleted second to fifth rows and columns in each block of $(b) + (c)$, we have shown that (63) holds. □

E. Proof of Theorem 1

Proof. From Proposition 4, $\dot{\mathcal{V}}(\hat{\mathbf{x}})$ is negative semidefinite ((26) holds). We show that the origin of the MG cluster is also attractive by using the LaSalle invariance Theorem [33]. For this purpose, the set $R = \{\mathbf{x} \in \mathbb{R}^{5N} : \mathbf{x}^T\mathbf{Q}\mathbf{x} = 0\}$ is first computed by means of the decomposition in (63), which coincides with

$$\begin{aligned} R &= \{\mathbf{x} : (\mathbf{x})^T((a) + (b) + (c))\,\mathbf{x} = 0\} \\ &= \{\mathbf{x} : (\mathbf{x})^T(a)\mathbf{x} + (\mathbf{x})^T(b)\mathbf{x} + (\mathbf{x})^T(c)\mathbf{x} = 0\} \\ &= \underbrace{\{\mathbf{x} : (\mathbf{x})^T(a)\mathbf{x} = 0\}}_{X_1} \cap \underbrace{\{\mathbf{x} : (\mathbf{x})^T[(b) + (c)]\,\mathbf{x} = 0\}}_{X_2}. \end{aligned} \quad (71)$$

In particular, the last equality follows from the fact that matrix (a) and $(b) + (c)$ are negative semidefinite matrices based on the proof of Propositions 2 and 4.

First, we characterize the set X_1. By exploiting Proposition 3, it follows that

$$X_1 = \{\mathbf{x} : \mathbf{x} = [\ \alpha_1\ 0\ \gamma_1\ \beta_1\ \delta_1\beta_1 |\ \cdots\ |\ \alpha_N\ 0\ \gamma_N\ \beta_N\ \delta_N\beta_N\ ]^T, \quad \alpha_i, \gamma_i, \beta_i \in \mathbb{R}\}, \quad (72)$$

Then, the elements of set X_2 can be characterized using Proposition 4. Since matrix $(b) + (c)$ can be seen as an 'expansion' of a matrix which is negative definite with zero entries on the second to fifth rows and columns of each 5×5 block. By construction, the vectors is in the form as

$$X_2 = \{\mathbf{x} : \mathbf{x} = [\ 0\ \tilde{x}_{12}\ \tilde{x}_{13}\ \tilde{x}_{14}\ \tilde{x}_{15}\ |\ \cdots\ |\ 0\ \tilde{x}_{N2}\ \tilde{x}_{N3}\ \tilde{x}_{N4}\ \tilde{x}_{N5}\ ]^T, \quad \tilde{x}_{i2}, \tilde{x}_{i3}, \tilde{x}_{i4}, \tilde{x}_{i5} \in \mathbb{R}\}, \quad (73)$$

Hence, by merging (72) and (73), it derives that

$$R = \{\mathbf{x} : \mathbf{x} = [\ 0\ 0\ \gamma_1\ \beta_1\ \delta_1\beta_1 |\ |\ \cdots\ |\ 0\ 0\ \gamma_N\ \beta_N\ \delta_N\beta_N |\ ]^T, \quad \gamma_i, \delta_i, \beta_i \in \mathbb{R}\}. \quad (74)$$

To conclude the proof, it should be shown that the largest invariant set $M \subseteq R$ is the origin. To this purpose, we consider (13), include coupling terms $\hat{\xi}_{[i]}$, resistive load term $\hat{A}_{load,i}\hat{x}_i(0)$; set $\hat{d}_{[i]} = 0$ and choose $\hat{\mathbf{x}}(0) = [\hat{x}_1(0)|\ldots|\hat{x}_N(0)]^T \in R$ as initial state. We aim to find

This article has been accepted for publication in a future issue of this journal, but has not been fully edited. Content may change prior to final publication. Citation information: DOI 10.1109/TPWRS.2018.2884876, IEEE Transactions on Power Systems

conditions on the elements of $\hat{\mathbf{x}}(0)$ that must hold for having $\dot{\hat{\mathbf{x}}} \in R$. One has

$$\begin{aligned}
\dot{\hat{x}}_i(0) &= F_i\hat{x}_i(0) + \hat{A}_{load,i}\hat{x}_i(0) + \sum_{j\in\mathcal{N}_i}\underbrace{\hat{A}_{ij}\left(\hat{x}_j(0)-\hat{x}_i(0)\right)}_{=0} \\
&= \left[\begin{array}{c|cc|cc}
-\frac{1}{R_{Li}C_{ti}} & \frac{1}{C_t} & 0 & \frac{1}{C_t} & 0 \\ \hline
\frac{(k^C_{1,i}-1)}{L^C_{ti}} & \frac{(k^C_{2,i}-R^C_{ti})}{L^C_{ti}} & \frac{k^C_{3,i}}{L^C_{ti}} & 0 & 0 \\
0 & -1 & 0 & 0 & 0 \\ \hline
\frac{(k^V_{1,i}-1)}{L^V_{ti}} & 0 & 0 & \frac{(k^V_{2,i}-R^V_{ti})}{L^V_{ti}} & \frac{k^V_{3,i}}{L^V_{ti}} \\
-1 & 0 & 0 & 0 & 0
\end{array}\right]\left[\begin{array}{c} 0 \\ 0 \\ \gamma_i \\ \beta_i \\ \delta_i\beta_i \end{array}\right] \\
&= \left[\begin{array}{c} \frac{\beta_i}{C_{ti}} \\ \frac{k^C_{3,i}}{L^C_{ti}}\gamma_i \\ 0 \\ \underbrace{\frac{k^V_{2,i}-R^V_{ti}}{L^V_{ti}}\beta_i + \frac{k^V_{3,i}}{L^V_{ti}}\delta_i\beta_i}_{=0} \\ 0 \end{array}\right] = \left[\begin{array}{c} \frac{\beta_i}{C_{ti}} \\ \frac{k^C_{3,i}}{L^C_{ti}}\gamma_i \\ 0 \\ 0 \\ 0 \end{array}\right]
\end{aligned}$$

for all $i \in \mathcal{D}$. It follows that $\dot{\hat{\mathbf{x}}}(0) \in R$ only if $\beta_i = 0$ and $\gamma_i = 0$. Since $M \subseteq R$, from (74) one has $M = \{0\}$. □

F. Proof of Lemma 3

Proof. Each vector $x \in \mathbb{R}^n$ can always be written in a unique way as [22]

$$x = \hat{x} + \bar{x} \text{ with } \hat{x} \in H^1 \text{ and } \bar{x} \in H^1_\perp \tag{75}$$

Then, one has

$$x^T(L+G)x = \hat{x}^T L\hat{x} + x^T Gx \tag{76}$$

(76) is equivalent to the two following cases

$$\begin{cases}
\text{If } \hat{x} \neq 0,\ \underbrace{\hat{x}^T L\hat{x}}_{>0} + \underbrace{x^T Gx}_{\geq 0} > 0 & \text{(77a)} \\
\text{If } \hat{x} = 0,\ \underbrace{\bar{x}^T L\bar{x}}_{=0} + \underbrace{\bar{x}^T G\bar{x}}_{>0} > 0 & \text{(77b)}
\end{cases}$$

Thus, matrix $L+G$ is positive definite matrix. □

G. Proof of Corollary 1

Proof. We recall that if α is a scalar, A is positive definite matrix and I is unit matrix which is also positive definite matrix, from Woodbury matrix identity theory [34] , one has

$$\begin{aligned}
&[I+\alpha A]^{-1} \\
&= \alpha^{-1}A^{-1} - \alpha^{-1}A^{-1}(\alpha^{-1}A^{-1}+I)^{-1}\alpha^{-1}A^{-1}
\end{aligned} \tag{78}$$

□

H. Proof of Lemma 5

Proof. From Corollary 1, matrix $[I + K_{pV}(L+G)]^{-1}$ is positive. Then, from (78), one has

$$\begin{aligned}
&(L+G)[I+K_{pV}(L+G)]^{-1} \\
&= K_{pV}^{-1}I - \left(K_{pV}^{-1}\right)^2\left[K_{pV}^{-1}(L+G)^{-1}+I\right]^{-1}(L+G)^{-1} \\
&= K_{pV}^{-1}I - \left(K_{pV}^{-1}\right)^2\left[K_{pV}^{-1}+(L+G)\right]^{-1}
\end{aligned} \tag{79}$$

Then

$$\begin{aligned}
&[I+K_{pV}(L+G)]^{-1}(L+G) \\
&= K_{pV}^{-1}I - \left(K_{pV}^{-1}\right)^2(L+G)^{-1}\left[K_{pV}^{-1}(L+G)^{-1}+I\right]^{-1} \\
&= K_{pV}^{-1}I - \left(K_{pV}^{-1}\right)^2\left[K_{pV}^{-1}+(L+G)\right]^{-1}
\end{aligned} \tag{80}$$

Comparing (79) with (80), we have

$$\begin{aligned}
&(L+G)[I+K_{pV}(L+G)]^{-1} \\
&= [I+K_{pV}(L+G)]^{-1}(L+G)
\end{aligned} \tag{81}$$

To conclude, from Lemma 4, since both matrices $(L+G)$ and $[I+K_{pV}(L+G)]^{-1}$ are positive definite, combined with (81), the matrix $(L+G)[I+K_{pV}(L+G)]^{-1}$ is positive definite. □